(MH$^+$). Found (FAB-HRMS): 713.3911. Calcd for $C_{37}H_{49}O_5N_{10}$ (MH$^+$): 713.3887.

***tert*-Butyl 2(*S*)-[[2(*S*)-[(*tert*-butoxy)carbonyamino]-5-[[imino[[(2,4,6-trimethylphenyl)sulfonyl]amino]methyl]-amino]pentyl]amino]-3-(2-naphthyl) Propanoate [Boc-L-Arg(Mts)-ψ[CH$_2$−NH]-L-Nal-O^{t}Bu], 26.** To a stirred solution of **25** (5.0 g, 10 mmol) in toluene/CH_2Cl_2 (1:1 (v/v), 50 mL) was added dropwise a solution of DIBAL-H in toluene (1.0 M, 60 mL, 60 mmol) at −50 °C under argon, and the mixture was stirred for 4 h at −78 °C. The reaction was quenched with saturated aqueous citric acid at −78 °C, and the organic solvents were concentrated under reduced pressure. The residue was extracted with EtOAc, and the extract was washed successively with saturated aqueous citric acid and brine and dried over $MgSO_4$. Concentration under reduced pressure gave a crude aldehyde (Boc-Arg(Mts)-H), which was used in the following step without further purification. To the stirred solution of Boc-Arg(Mts)-H in $ClCH_2CH_2Cl$/DMF (1:6 (v/v), 100 mL), were added H-L-Nal-O^{t}Bu (5.4 g, 20 mmol) and AcOH (1.1 mL, 20 mmol) at 4 °C and stirred for 10 min. $NaBH(OAc)_3$ (6.4 g, 30 mmol) was added to the above mixture at 4 °C and stirred for 8 h with warming to room temperature. The mixture was concentrated under reduced pressure, and the residue was extracted with $CHCl_3$. The extract was washed with aqueous 5% $NaHCO_3$ and brine and dried over $MgSO_4$. Concentration under reduced pressure gave an oily residue, which was purified by chromatography over silica gel with $CHCl_3$/MeOH (39:1) to yield 3.4 g (4.9 mmol, 49% yield from **25**) of compound **26** as a yellow oil.

$[\alpha]^{23}_D$ 4.08 (*c* 1.96, $CHCl_3$). ^{1}H NMR (270 MHz, $CDCl_3$) δ: 1.24 (9H, s, *tert*-Bu), 1.32 (9H, s, *tert*-Bu), 1.55 (2H, br m, 4-CH_2), 1.74 (2H, br m, 3-CH_2), 2.25 (3H, s, Ar-*p*-Me), 2.67 (6H, s, Ar-*o*-Me), 3.08 (2H, br m, 5-CH_2), 3.20 (2H, br, 3-CH_2), 3.34 (2H, br, 1-CH_2), 3.62 (1H, br, 2-H), 3.82 (1H, br, 2-H), 3.99 (1H, br, NH), 5.95 (1H, br, NH), 6.61 (3H, br, guanidino), 6.87 (2H, s, Ar-*m*-H), 7.36−7.44 (3H, m, ArH), 7.67−7.75 (4H, m, ArH). *m/z* (ISMS): 697.0 (MH$^+$). Found (FAB-HRMS): 696.3812. Calcd for $C_{37}H_{54}O_6N_5S$ (MH$^+$): 696.3795.

***tert*-Butyl 2(*S*)-[*N*-[2(*S*)-[(*tert*-Butoxy)carbonylamino]-5-[[imino[[(2,4,6-trimethylphenyl)sulfonyl]amino]methyl]-amino]pentyl](phenylmethoxy)carbonylamino]-3-(2-naphthyl)propanoate [Boc-Arg(Mts)-ψ[CH$_2$−N(Cbz)]-Nal-O^{t}Bu], 27.** To a stirred solution of propanoate **26** (1.4 g, 2.0 mmol) in DMF (100 mL) at 4 °C, were added Cbz-Cl (0.69 g, 4.0 mmol) and Et_3N (560 μL, 4.0 mmol) and stirred at room temperature for 8 h. The mixture was concentrated under reduced pressure and extracted with EtOAc. The extract was washed with saturated aqueous citric acid, saturated aqueous $NaHCO_3$, and brine and dried over $MgSO_4$. Concentration under reduced pressure followed by chromatography over silica gel with EtOAc/*n*-hexane (1:1) gave the title compound **27** (1.6 g, 77% yield from **26**) as a yellow oil.

$[\alpha]^{23}_D$ −36.44 (*c* 0.67, $CHCl_3$). ^{1}H NMR (270 MHz, $CDCl_3$) δ: 1.39 (9H, s, *tert*-Bu), 1.42 (9H, s, *tert*-Bu), 1.47 (2H, s, 4-CH_2), 1.64 (2H, br, 3-CH_2), 2.42 (3H, s, Ar-*p*-Me), 2.65 (6H, s, Ar-*o*-Me), 2.98 (2H, br, 5-CH_2), 3.27 (2H, br, 3-CH_2), 3.31 (2H, br, 1-CH_2), 3.40 (1H, br, 2-H), 4.24 (1H, br, 2-H), 5.08 (2H, s, CH_2), 5.90 (1H, br, NH), 6.13 (3H, br, guanidino), 6.86 (2H, s, Ar-*m*-H), 7.26 (5H, s, ArH), 7.31−7.46 (3H, m, ArH), 7.54−7.75 (4H, m, ArH). *m/z* (ISMS): 831.5 (MH$^+$). Found (FAB-HRMS): 830.4153. Calcd for $C_{45}H_{60}O_8N_5S$ (MH$^+$): 830.4163.

2(*S*)-[*N*-[2(*S*)-[(Fluoren-9-ylmethoxy)carbonylamino]-5-[[imino[[(2,4,6-trimethylphenyl)sulfonyl]amino]methyl]-amino]pentyl](phenylmethoxy)carbonylamino]-3-(2-naphthyl)propanoic Acid [Fmoc-Arg(Mts)-ψ[CH$_2$−N(Cbz)]-Nal-OH], 28. The propanoate **27** (1.3 g, 1.57 mmol) was dissolved in TFA (30 mL), anisole (170 μL, 1.57 mmol) was added to the solution at 4 °C, and the mixture was stirred at room temperature for 2 h. The mixture was concentrated under reduced pressure and dissolved in THF and H_2O (1:1 (v/v) 100 mL). To the stirred solution were added Fmoc-OSu (530 mg, 1.57 mmol) and Et_3N (10 mL, 71.7 mmol) at 4 °C, and the mixture was stirred at room temperature for 8 h. The mixture was acidified with aqueous 1 M HCl and extracted with EtOAc. The extract was washed with aqueous 0.1 M HCl and brine and dried over $MgSO_4$. Concentration under reduced pressure followed by chromatography over silica gel with EtOAc/*n*-hexane (4:1) gave the propanoic acid **28** (1.39 g, 99% yield from **27**) as white crystals.

Mp: 156−158 °C (from *n*-hexane). $[\alpha]^{24}_D$ −8.17 (*c* 1.96, $CHCl_3$). ^{1}H NMR (270 MHz, $CDCl_3$) δ: 1.85 (2H, br, 4-CH_2), 1.93 (2H, br, 3-CH_2), 2.11 (3H, s, Ar-*p*-Me), 2.47 (6H, s, Ar-*o*-Me), 3.03 (2H, br, 5-CH_2), 3.22 (2H, br, 3-H), 3.37 (2H, br, 1-CH_2), 4.08 (1H, br, ArH), 4.15 (2H, br, CH_2), 4.30 (1H, br, 2-H), 5.16 (1H, br, NH), 6.36 (3H, br, guanidino), 6.83 (2H, s, Ar-*m*-H) 7.25 (5H, s, ArH), 7.29−7.40 (6H, m, ArH), 7.50−7.83 (9H, m, ArH). *m/z* (ISMS): 897.0 (MH$^+$). Found (FAB-HRMS): 896.3693. Calcd for $C_{51}H_{54}O_8N_5S$ (MH$^+$): 896.3710.

H-D-Tyr(O^{t}Bu)-Arg(Pbf)-Arg(Mts)-ψ[CH$_2$−NH]-Nal-Gly-NHNHCO−Wang Resin. On the hydrazide resin were coupled successively Fmoc-Gly-OH, Fmoc-Arg-ψ[CH$_2$−N(Cbz)]-Nal-OH, Fmoc-Arg(Pbf)-OH, and Fmoc-D-Tyr(O^{t}Bu)-OH by use of a procedure identical with that described for the preparation of H-D-Tyr(O^{t}Bu)-Arg(Pbf)-Arg(Mts)-ψ[(*E*)-CH=CH]-Nal-Gly-NHNHCO−Wang resin to afford the protected **37b** resin.

***cyclo*(-D-Tyr-Arg-Arg-ψ[CH$_2$−NH]-Nal-Gly-)·3TFA (37b).** By use of a procedure identical with that described for the preparation of **37a**, the protected **37b** (200 mg, 0.15 mmol) was converted into 0.6 mg (0.57 μmol, 0.86%) of the title compound **37b**, as a freeze-dried powder.

$[\alpha]^{21}_D$ −22.6 (*c* 0.27, H_2O). t_R = 19.3 min (linear gradient of MeCN in H_2O, 10 to 40% over 30 min). *m/z* (ISMS): 717.0 (MH$^+$). Found (FAB-HRMS): 716.4016. Calcd for $C_{36}H_{49}O_5N_{11}$ (MH$^+$): 716.3996.

***tert*-Butyl 2(*S*)-[[2-[(*tert*-Butoxy)carbonylamino]-3-(2-naphthyl)propyl]amino]acetate [Boc-L-Nal-ψ[CH$_2$−NH]-Gly-O^{t}Bu], 30.** To a stirred solution of Boc-Nal-NMe(OMe) **29** (5.5 g, 15 mmol) in toluene/CH_2Cl_2 (1:1 (v/v) 50 mL) was added dropwise a solution of DIBAL-H in toluene (1.0 M, 62 mL, 62 mmol) at −78 °C under argon, and the mixture was stirred at −78 °C for 4 h. The reaction was quenched with saturated aqueous citric acid at −78 °C, and organic solvents were concentrated under reduced pressure. The residue was extracted with EtOAc, and the extract was washed successively with saturated aqueous citric acid and brine and dried over $MgSO_4$. Concentration under reduced pressure gave a crude aldehyde (Boc-Nal-H), which was used in the following step without further purification. To the stirred solution of Boc-Nal-H in $ClCH_2CH_2Cl$/DMF (1:6 (v/v), 200 mL), was added H-Gly-O^{t}Bu·AcOH (5.8 g, 31 mmol) at 4 °C and stirred for 10 min. $NaBH(OAc)_3$ (9.8 g, 46 mmol) was added to the above mixture at 4 °C and stirred for 8 h with warming to room temperature. The mixture was concentrated under reduced pressure, and the residue was extracted with $CHCl_3$. The extract was washed with aqueous 5% $NaHCO_3$ and brine and dried over $MgSO_4$. Concentration under reduced pressure gave an oily residue, which was purified by chromatography over silica gel with $CHCl_3$ to yield 3.2 g (7.7 mmol, 50% yield from **29**) of compound **30** as a yellow oil.

$[\alpha]^{22}_D$ −0.67 (*c* 4.47, $CHCl_3$). ^{1}H NMR (400 MHz, $CDCl_3$) δ: 1.38 (9H, s, *tert*-Bu), 1.47 (9H, s, *tert*-Bu), 2.87 (2H, br, CH_2), 3.02 (2H, br, 3-CH_2), 3.85−3.94 (2H, m, 1-CH_2), 4.09−4.21 (1H, m, 2-H), 5.44 (1H, br, NH), 6.45 (1H, br, NH), 7.29−7.36 (2H, m, Ar−H), 7.41−7.48 (2H, m, ArH), 7.60−7.62 (1H, m, ArH), 7.72−7.83 (2H, m, ArH). *m/z* (ISMS): 415.5 (MH$^+$). Found (FAB-HRMS): 415.2594. Calcd for $C_{24}H_{35}O_4N_2$ (MH$^+$): 415.2597.

***tert*-Butyl 2(*S*)-[*N*-[2-[(*tert*-Butoxy)carbonylamino]-3-(2-naphthyl)propyl](phenylmethoxy)carbonylamino]acetate [Boc-L-Nal-ψ[CH$_2$−N(Cbz)]-Gly-O^{t}Bu], 31.** To a stirred solution of acetate **30** (5.0 g, 12.1 mmol) in DMF (100 mL) at 4 °C were added Cbz-Cl (20.6 g, 121 mmol) and DIPEA (21.7 mL, 121 mmol), and the mixture was stirred at room temperature for 8 h. The mixture was concentrated under reduced pressure and extracted with EtOAc. The solution was washed with saturated aqueous citric acid, saturated aqueous $NaHCO_3$, and brine and dried over $MgSO_4$. Concentration under

reduced pressure followed by chromatography over silica gel with EtOAc/*n*-hexane (1:2) gave the title compound **31** (4.0 g, 60% yield from **30**) as white crystals.

Mp: 107−109 °C (from *n*-hexane). Found: C, 70.01; H, 7.42 N, 4.98. Calcd for $C_{32}H_{40}O_6N_2$: C, 70.05; H, 7.35; N, 5.11. $[\alpha]^{23}_D$ −14.73 (*c* 0.48, $CHCl_3$). ^1H NMR (400 MHz, $CDCl_3$) δ: 1.34 (9H, s, *tert*-Bu), 1.35 (9H, s, *tert*-Bu), 2.94 (2H, br, CH_2), 3.37 (2H, br, 3-CH_2), 3.88 (2H, m, 1-CH_2), 4.05 (1H, m, 2-H), 4.94 (1H, br, NH), 5.13 (2H, s, CH_2), 7.28−7.33 (5H, br, ArH), 7.35−7.47 (3H, m, ArH), 7.74−7.81 (4H, m, ArH). *m/z* (ISMS): 549.5 (MH^+). Found (FAB-HRMS): 549.2953. Calcd for $C_{32}H_{41}O_6N_2$ (MH^+): 549.2965.

2(*S*)-[*N*-[2-[(Fluoren-9-ylmethoxy)carbonylamino]-3-(2-naphthyl)propyl](phenylmethoxy)carbonylamino]-acetic Acid [Fmoc-L-Nal-ψ[CH_2−N(Cbz)]-Gly-OH], 32. The acetate **31** (4.0 g, 7.29 mmol) was dissolved in TFA (30 mL), anisole (792 μL, 7.29 mmol) was added to the solution at 4 °C, and the mixture was stirred at room temperature for 2 h. The mixture was concentrated under reduced pressure and dissolved in THF and H_2O (1:1 (v/v) 100 mL). To the stirred solution, were added Fmoc-OSu (2.46 g, 7.29 mmol) and Et_3N (10 mL, 71.7 mmol) at 4 °C, and the mixture was stirred at room temperature for 8 h. The mixture was acidified with aqueous 1 M HCl and was extracted with EtOAc. The extract was washed with aqueous 0.1 M HCl and brine and dried over $MgSO_4$. Concentration under reduced pressure followed by chromatography over silica gel with $CHCl_3$/MeOH (39:1) gave the title compound **32** (4.20 g, 94% yield from **31**) as a yellow oil.

$[\alpha]^{23}_D$ −5.01 (*c* 4.79, $CHCl_3$). ^1H NMR (400 MHz, $CDCl_3$) δ: 2.99 (2H, d, J = 6.4 Hz, 3-CH_2), 3.41 (2H, s, CH_2), 4.00 (2H, br, 1-CH_2), 4.08 (1H, t, J = 6.6 Hz, Ar−H), 4.24 (1H, t, J = 6.2 Hz, 2-H), 4.27 (2H, br, CH_2), 5.05 (2H, s, CH_2), 5.53 (1H, d, J = 8.0 Hz, NH), 7.18 (5H, s, Ar−H) 7.30−7.50 (8H, m, ArH), 7.61−7.73 (7H, m, ArH). *m/z* (ISMS): 615.0 (MH^+). Found (FAB-HRMS): 615.2509. Calcd for $C_{38}H_{35}O_6N_2$ (MH^+): 615.2495.

H-D-Tyr(O^{t}Bu)-Arg(Pbf)-Arg(Pbf)-Nal-ψ[CH_2−N(Cbz)]-Gly-NHNHCO−Wang Resin. On the hydrazide resin, were coupled successively Fmoc-D-Tyr(O^{t}Bu)-OH, Fmoc-Nal-ψ[CH_2−N(Cbz)]-Gly-OH, and Fmoc-Arg(Pbf)-OH by use of a procedure identical with that described for the preparation of H-D-Tyr-(O^{t}Bu)-Arg(Pbf)-Arg(Mts)-ψ[(*E*)-CH=CH]-Nal-Gly-NHNHCO−Wang resin to afford the protected **37d** resin.

***cyclo*(-D-Tyr-Arg-Arg-Nal-ψ[CH_2−NH]-Gly-)·3TFA (37d).** By use of a procedure identical with that described for the preparation of **37a**, the protected **37d** (173 mg, 0.13 mmol) was converted into 7.0 mg (7.4 μmol, 5.9%) of the title compound **37d**, as a freeze-dried powder.

$[\alpha]^{19}_D$ −58.0 (*c* 0.69, H_2O). t_R = 21.0 min (linear gradient of MeCN in H_2O, 10 to 40% over 30 min). *m/z* (ISMS): 717.0 (MH^+). Found (FAB-HRMS): 716.4003. Calcd for $C_{36}H_{49}O_5N_{11}$ (MH^+): 716.3996.

Cell Culture. Human T-cell lines, MT-4, and MOLT-4 cells were grown in RPMI 1640 medium containing 10% heat-inactivated fetal calf serum, 100 IU/mL penicillin, and 100 μg/mL streptomycin.

Virus. A strain of X4-HIV-1, HIV-1$_{IIIB}$, was used for the anti-HIV assay. This virus was obtained from the culture supernatant of HIV-1 persistently infected MOLT-4/HIV-1$_{IIIB}$ cells and stored at −80 °C until used.

Anti-HIV-1 Assay. Anti-HIV-1 activity was determined based on the protection against HIV-1-induced cytopathogenicity in MT-4 cells. Various concentrations of test compounds were added to HIV-1-infected MT-4 cells at a multiplicity of infection (MOI) of 0.01 and placed in wells of a flat-bottomed microtiter tray (1.5 × 10^4 cells/well). After 5 days incubation at 37 °C in a CO_2 incubator, the number of viable cells was determined using the 3-(4,5-dimethylthiazol-2-yl)-2,5-diphenyltetrazolium bromide (MTT) method (EC_{50}).[48] Cytotoxicity of compounds was determined based on the viability of mock-infected cells using the MTT method (CC_{50}). 3′-Azido-3′-dideoxythymidine (AZT) was tested as a control.

[^{125}I]-SDF-1 Binding and Displacement. Stable CHO cell transfectants expressing CXCR4 variants were prepared as described previously.[49] CHO transfectants were harvested by treatment with trypsin/EDTA, allowed to recover in complete growth medium (MEM-α, 100 μg/mL penicillin, 100 μg/mL streptomycin, 0.25 μg/mL amphotericin B, 10% (v/v)) for 4−5 h, and then washed in cold binding buffer (PBS containing 2 mg/mL BSA). For ligand binding, the cells were resuspended in binding buffer at 1 × 10^7 cells/mL, and 100 μL aliquots were incubated with 0.1 nM of [^{125}I]-SDF-1 (PerkinElmer Life Sciences) for 2 h on ice under constant agitation. Free and bound radioactivities were separated by centrifugation of the cells through an oil cushion, and bound radioactivity was measured with a gamma counter (Cobra, Packard, Downers Grove, IL). Inhibitory activity of FC131 analogues was determined based on the inhibition of [^{125}I]-SDF-1-binding to CXCR4 transfectants (IC_{50}).

NMR Spectroscopy (37a and 37c). The peptide sample was dissolved in DMSO-d_6 at a concentration of 5 mM. ^1H NMR spectra of the peptides were recorded at 300 K. The assignments of the proton resonances were achieved by use of ^1H−^1H COSY spectra. $^3J(H^N, H^\alpha)$ coupling constants were measured from one-dimensional spectra. The mixing time for the nuclear Overhauser spectroscopy (NOESY) experiments was set at 400 ms. NOESY spectra were composed of 512 real points in the F2 dimension and 256 real points, which were zero-filled to 256 points in the F1 dimension, with 144 scans per t1 increment. The cross-peak intensities were evaluated by relative buildup rates of the cross peaks. Temperature dependence of the chemical shifts of all of the amide bonds was investigated in **37a** and **37c**. The only temperature coefficient for the NH of Arg^5 was small, but NOE was not observed between the D-Tyr^3 C$^\alpha$H and the Arg^5 NH in both **37a** and **37c**. Thus, no hydrogen bond restraints were used in the simulated annealing calculations.

Calculation of Structures. The structure calculations were performed on a Silicon Graphics Origin 2000 workstation with the NMR refine program within the Insight II/Discover package using the consistent valence force field (CVFF).[51] Pseudoatoms were defined for the methylene protons of Nal^1, D-Tyr^3, Arg^4, and Arg^5, prochiralities of which were not identified by ^1H NMR data. The restraints, in which the Gly^2 α-methylene participated, were defined for the separate protons without definition of the prochiralities. The dihedral ϕ angle constraints were calculated based on the Karplus equation: $^3J(H^N,H^\alpha) = 6.7\cos^2(\theta - 60°) - 1.3\cos(\theta - 60°) + 1.5$.[52] Lower and upper angle errors were set to 15°. The NOESY spectrum with a mixing time of 400 ms was used for the estimation of the distance restraints between protons. The NOE intensities were classified into three categories (strong, medium, and weak) based on the number of contour lines in the cross peaks to define the upper-limit distance restraints (2.7, 3.5, and 5.0 Å, respectively). The upper-limit restraints were increased by 1.0 Å for the involved pseudoatoms. Lower bounds between nonbonded atoms were set to their van der Waals radii (1.8 Å). These distance and dihedral angle restraints were included with force constants of 25−100 kcal/mol·Å^2 and 25−100 kcal/mol·rad^2, respectively. The 50 initial structures generated by the NMR refine program randomly were subjected to the simulated annealing calculations. The final minimization stage was achieved until the maximum derivative became less than 0.01 kcal/mol·Å^2 by the steepest descents and conjugate gradients methods.

Acknowledgment. This work was supported in part by a 21st Century COE Program "Knowledge Information Infrastructure for Genome Science", a Grant-in-Aid for Scientific Research from the Ministry of Education, Culture, Sports, Science and Technology, Japan and the Japan Health Science Foundation. Computation time was provided by the Supercomputer Laboratory, Institute for Chemical Research, Kyoto University. S.U. is

grateful for a Research Fellowship from the Japan Society for the Promotion of Science for Young Scientists.

Supporting Information Available: HPLC charts for synthetic compounds of **37a**, **37b**, **37c**, **37d**, and **37f**. These materials are available free of charge via the Internet at http://pubs.acs.org.

References

(1) Kaltenbronn, J. S.; Hudspeth, J. P.; Lunney, E. A.; Michniewicz, B. M.; Nicolaides, E. D.; Repine, J. T.; Roark, W. H.; Stier, M. A.; Tinney, F. J.; Woo, P. K. W.; Essenburg, A. D. Renin inhibitors containing isosteric replacements of the amide bond connecting the P_3 and P_2 sites. *J. Med. Chem.* **1990**, *33*, 838–845.

(2) Ibuka, T.; Habashita, H.; Otaka, A.; Fujii, N. A highly stereoselective synthesis of (*E*)-alkene dipeptide isosteres via organocyanocopper–lewis acid mediated reaction. *J. Org. Chem.* **1991**, *56*, 4370–4382.

(3) Wipf, P.; Fritch, P. C. S_N2' reactions of peptide aziridines. A cuprate-based approach to (*E*)-alkene isosteres. *J. Org. Chem.* **1994**, *59*, 4875–4886.

(4) Fujii, N.; Nakai, K.; Tamamura, H.; Otaka, A.; Mimura, N.; Miwa, Y.; Taga, T.; Yamamoto, Y.; Ibuka, T. S_N2' ring opening of aziridines bearing an α,β-unsaturated ester group with organocopper reagents. A new stereoselective synthetic route to (*E*)-alkene dipeptide isosteres. *J. Chem. Soc., Perkin Trans. 1* **1995**, 1359–1371.

(5) Daly, M. J.; Ward, R. A.; Thompson, D. F.; Procter, G. Allylsilanes in organic synthesis; stereoselective synthesis of *trans*-alkene peptide isosteres. *Tetrahedron Lett.* **1995**, *36*, 7545–7548.

(6) Tamamura, H.; Hiramatsu, K.; Miyamoto, K.; Omagari, A.; Oishi, S.; Nakashima, H.; Yamamoto, N.; Kuroda, Y.; Nakagawa, T.; Otaka, A.; Fujii, N. Synthesis and evaluation of pseudopeptide analogues of a specific CXCR4 inhibitor, T140: The insertion of an (*E*)-alkene dipeptide isostere into the βII′-turn moiety. *Bioorg. Med. Chem. Lett.* **2002**, *12*, 923–928.

(7) Tamamura, H.; Koh, Y.; Ueda, S.; Sasaki, Y.; Yamasaki, T.; Aoki, M.; Maeda, K.; Watai, Y.; Arikuni, H.; Otaka, A.; Mitsuya, H.; Fujii, N. Reduction of peptide character of HIV protease inhibitors that exhibit nanomolar potency against multi-drug resistant HIV-1 strains. *J. Med. Chem.* **2003**, *46*, 1764–1768.

(8) Tamamura, H.; Yamashita, M.; Muramatsu, H.; Ohno, H.; Ibuka, T.; Otaka, A.; Fujii, N. Regiospecific ring-opening reactions of aziridines bearing an α,β-unsaturated ester group with trifluoroacetic acid or methanesulfonic acid: Application to the stereoselective synthesis of (*E*)-alkene dipeptide isosteres. *Chem. Commun.* **1997**, 2327–2328.

(9) Tamamura, H.; Yamashita, M.; Nakajima, Y.; Sakano, K.; Otaka, A.; Ohno, H.; Ibuka, T.; Fujii, N. Regiospecific ring-opening reactions of β-aziridinyl α,β-enoates with acids: application to the stereoselective synthesis of a couple of diastereoisomeric (*E*)-alkene dipeptide isosteres from a single β-aziridinyl α,β-enoate and to the convenient preparation of amino alcohols bearing α,β-unsaturated ester groups. *J. Chem. Soc., Perkin Trans. 1*, **1999**, 2983–2996.

(10) Oishi, S.; Tamamura, H.; Yamashita, M.; Odagaki, Y.; Hamanaka, N.; Otaka, A.; Fujii, N. Stereoselective synthesis of a set of two functionalized (*E*)-alkene dipeptide isosteres of L-amino acid-L-Glu and L-amino acid-D-Glu. *J. Chem. Soc., Perkin Trans. 1* **2001**, 2445–2451.

(11) Nakamura, E.; Aoki, S.; Sekiya, K.; Oshino, H.; Kuwajima, I. Carbon–carbon bond-forming reactions of zinc homoenolate of esters. A novel three-carbon nucleophile with general synthetic utility. *J. Am. Chem. Soc.* **1987**, *109*, 8056–8066.

(12) Ochiai, H.; Tamaru, Y.; Tsubaki, K.; Yoshida, Z. Unsaturated ester synthesis via copper(I)-catalyzed allylation of zinc esters. *J. Org. Chem.* **1987**, *52*, 4418–4420.

(13) Yeh, M. C. P.; Knochel, P. 2-Cyanoethylzinc iodide: A new reagent with reactivity umpolung.*Tetrahedron Lett.* **1988**, *29*, 2395–2396.

(14) Knochel, P.; Yeh, M. C. P.; Berk, S. C.; Talbert, J. Synthesis and reactivity toward acyl chlorides and enones of the new highly functionalized copper reagents RCu(CN)ZnI. *J. Org. Chem.* **1988**, *53*, 2390–2392.

(15) Zhu, L.; Wehmeyer, R. M.; Rieke, R. D. The direct formation of functionalized alkyl(aryl)zinc halides by oxidative addition of highly reactive zinc with organic halides and their reactions with acid chlorides, α,β-unsaturated ketones, and allylic, aryl, and vinyl halides. *J. Org. Chem.* **1991**, *56*, 1445–1453.

(16) Fujii, N.; Oishi, S.; Hiramatsu, K.; Araki, T.; Ueda, S.; Tamamura, H.; Otaka, A.; Kusano, S.; Terakubo, S.; Nakashima, H.; Broach, J. A.; Trent, J. O.; Wang, Z.; Peiper, S. C. Molecular-size reduction of a potent CXCR4–chemokine antagonist using orthogonal combination of conformation- and sequence-based libraries. *Angew. Chem., Int. Ed.* **2003**, *42*, 3251–3253.

(17) Koshiba, T.; Hosotani, R.; Miyamoto, Y.; Ida, J.; Tsuji, S.; Nakajima, S.; Kawaguchi, M.; Kobayashi, H.; Doi, R.; Hori, T.; Fujii, N.; Imamura, M. Expression of stromal cell-derived factor 1 and CXCR4 ligand receptor system in pancreatic cancer: a possible role for tumor progression. *Clin. Cancer. Res.* **2000**, *6*, 3530–3535.

(18) Müller, A.; Homey, B.; Soto, H.; Ge, N.; Catron, D.; Buchanan, M. E.; McClanahan, T.; Murphy, E.; Yuan, W.; Wagner, S. N.; Barrera, J. L.; Mohar, A.; Verastegui, E.; Zlotnik, A. Involvement of chemokine receptors in breast cancer metastasis. *Nature* **2001**, *410*, 50–56.

(19) Tamamura, H.; Hori, A.; Kanzaki, N.; Hiramatsu, K.; Mizumoto, M.; Nakashima, H.; Yamamoto, N.; Otaka, A.; Fujii, N. T140 analogs as CXCR4 antagonists identified as anti-metastatic agents in the treatment of breast cancer. *FEBS Lett.* **2003**, *550*, 79–83.

(20) Feng, Y.; Broder, C. C.; Kennedy, P. E.; Berger, E. A. HIV-1 entry co-factor: Functional cDNA cloning of a seven-transmembrane, G protein-coupled receptor. *Science* **1996**, *272*, 872–877.

(21) Nanki, T.; Hayashida, K.; El–Gabalawy, H. S.; Suson, S.; Shi, K.; Girschick, H. J.; Yavuz, S.; Lipsky, P. E. Stromal cell-derived factor-1-CXC chemokine receptor interactions play a central role in $CD4^+$ T cell accumulation in rheumatoid arthritis synovium. *J. Immunol.* **2000**, *165*, 6590–6598.

(22) Tamamura, H.; Fujisawa, M.; Hiramatsu, K.; Mizumoto, M.; Nakashima, H.; Yamamoto, N.; Otaka, A.; Fujii, N. Identification of a CXCR4 antagonist, a T140 analog, as an anti-rheumatoid arthritis agent. *FEBS Lett.* **2004**, *569*, 99–104.

(23) Murakami, T.; Nakajima, T.; Koyanagi, Y.; Tachibana, K.; Fujii, N.; Tamamura, H.; Yoshida, N.; Waki, M.; Matsumoto, A.; Yoshie, O.; Kishimoto, T.; Yamamoto, N.; Nagasawa, T. A small molecule CXCR4 inhibitor that blocks T cell line-tropic HIV-1 infection. *J. Exp. Med.*, **1997**, *186*, 1389–1393.

(24) Schols, D.; Struyf, S.; Van Damme, J.; Este, J. A.; Henson, G.; De Clercq, E. Inhibition of T-tropic HIV strains by selective antagonization of the chemokine receptor CXCR4. *J. Exp. Med.* **1997**, *186*, 1383–1388.

(25) Donzella, G. A.; Schols, D.; Lin, S. W.; Este J. A.; Nagashima, K. A.; Maddon, P. J.; Allaway, G. P.; Sakmar, T. P.; Henson, G.; De Clercq, E.; Moore, J. P. AMD3100, a small molecule inhibitor of HIV-1 entry via the CXCR4 co-receptor. *Nat. Med.* **1998**, *4*, 72–77.

(26) Doranz, B. J.; Grovit-Ferbas, K.; Sharron, M. P.; Mao, S.-H.; Bidwell Goetz, M.; Daar, E. S.; Doms, R. W.; O'Brien, W. A. A small-molecule inhibitor directed against the chemokine receptor CXCR4 prevents its use as an HIV-1 coreceptor. *J. Exp. Med.* **1997**, *186*, 1395–1400.

(27) Howard, O. M. Z.; Oppenheim, J. J.; Hollingshead, M. G.; Covey, J. M.; Bigelow, J.; McCormack, J. J.; Buckheit, Jr., R. W.; Clanton, D. J.; Turpin, J. A.; Rice, W. G. Inhibition of in vitro and in vivo HIV replication by a distamycin analogue that interferes with chemokine receptor function: a candidate for chemotherapeutic and microbicidal application. *J. Med. Chem.* **1998**, *41*, 2184–2193.

(28) Tamamura, H.; Xu, Y.; Hattori, T.; Zhang, X.; Arakaki, R.; Kanbara, K.; Omagari, A.; Otaka, A.; Ibuka, T.; Yamamoto, N.; Nakashima, H.; Fujii, N. A low molecular weight inhibitor against the chemokine receptor CXCR4: a strong anti-HIV peptide T140. *Biochem. Biophys. Res. Commun.* **1998**, *253*, 877–882.

(29) Tamamura, H.; Omagari, A.; Oishi, S.; Kanamoto, T.; Yamamoto, N.; Peiper, S. C.; Nakashima, H.; Otaka, A.; Fujii, N. Pharmacophore identification of a specific CXCR4 inhibitor, T140, leads to development of effective anti-HIV agents with very high selectivity indexes. *Bioorg. Med. Chem. Lett.* **2000**, *10*, 2633–2637.

(30) Fujii, N.; Nakashima, H.; Tamamura, H. The therapeutic potential of CXCR4 antagonists in the treatment of HIV. *Expert Opin. Invest. Drugs* **2003**, *12*, 185–195.

(31) Fukami, T.; Nagase, T.; Fujita, K.; Hayama, T.; Niiyama, K.; Mase, T.; Nakajima, S.; Fukuroda, T.; Saeki, T.; Nishikibe, M.; Ihara, M.; Yano, M.; Ishikawa, K. Structure–activity relationships of cyclic pentapeptide endothelin A receptor antagonists. *J. Med. Chem.* **1995**, *38*, 4309–4324.

(32) Haubner, R.; Gratias, R.; Diefenbach, B.; Goodman, S. L.; Jonczyk, A.; Kessler, H. Structural and functional aspects of RGD-containing cyclic pentapeptides as highly potent and selective integrin $\alpha V\beta 3$ antagonists. *J. Am. Chem. Soc.* **1996**, *118*, 7461–7472.

(33) Spatola, A. F.; Crozet, Y.; deWit, D.; Yanagisawa, M. Rediscovering an endothelin antagonist (BQ-123): A self-deconvoluting cyclic pentapeptide library. *J. Med. Chem.* **1996**, *39*, 3842−3846.
(34) Wermuth, J.; Goodman, S. L.; Jonczyk, A.; Kessler, H. Stereoisomerism and biological activity of the selective and superactive αVβ3 integrin inhibitor cyclo(−RGDfV-) and its retro-inverso peptide. *J. Am. Chem. Soc.* **1997**, *119*, 1328−1335.
(35) Haubner, R.; Finsinger, D.; Kessler, H. Stereoisomeric peptide libraries and peptidomimetics for designing selective inhibitors of the αVβ3 integrin for a new cancer therapy. *Angew. Chem., Int. Ed. Engl.* **1997**, *36*, 1374−1389.
(36) Porcelli, M.; Casu, M.; Lai, A.; Saba, G.; Pinori, M.; Cappelletti, S.; Mascagni, P. Cyclic pentapeptides of chiral sequence DLDDL as scaffold for antagonism of G-protein coupled receptors: Synthesis, activity and conformational analysis by NMR and molecular dynamics of ITF 1565 a substance P inhibitor. *Biopolymers* **1999**, *50*, 211−219.
(37) Oishi, S.; Kamano, T.; Niida, A.; Odagaki, Y.; Hamanaka, N.; Yamamoto, M.; Ajito, K.; Tamamura, H.; Otaka, A.; Fujii, N. Diastereoselective synthesis of new ψ[[(*E*)-CH=CMe]- and ψ[[(*Z*)-CH=CMe]-type alkene dipeptide isosteres by organocopper reagents and application to conformationally restricted cyclic RGD peptidomimetics. *J. Org. Chem.* **2002**, *67*, 6162−6173.
(38) Tamamura, H.; Hiramatsu, K.; Kusano, S.; Terakubo, S.; Yamamoto, N.; Trent, J. O.; Wang, Z.; Peiper, S. C.; Nakashima, H.; Otaka, A.; Fujii, N. Synthesis of potent CXCR4 inhibitors possessing low cytotoxicity and improved biostability based on T140 derivatives. *Org. Biomol. Chem.* **2003**, *1*, 3656−3662.
(39) Tamamura, H.; Hiramatsu, K.; Mizumoto, M.; Ueda, S.; Kusano, S.; Terakubo, S.; Akamatsu, M.; Yamamoto, N.; Trent, J. O.; Wang, Z.; Peiper, S. C.; Nakashima, H.; Otaka, A.; Fujii, N. Enhancement of the T140-based pharmacophores leads to the development of more potent and bio-stable CXCR4 antagonists. *Org. Biomol. Chem.* **2003**, *1*, 3663−3669.
(40) Inagawa, J.; Ishikawa, M.; Yamaguchi, M. A mild and convenient method for the reduction of organic halides by using a SmI_2-THF solution in the presence of hexamethylphosphoric triamide (HMPA). *Chem. Lett.* **1987**, 1485−1486.
(41) Otaka, A.; Yukimasa, A.; Watanabe, J.; Sasaki, Y.; Oishi, S.; Tamamura, H.; Fujii, N. Application of samarium diiodide (SmI_2)-induced reduction of γ-acetoxy-α,β-enoates with α-specific kinetic electrophilic trapping for the synthesis of amino acid derivatives. *Chem. Commun.* **2003**, 1834−1835.
(42) Fukuyama, T.; Jow, C. K.; Cheng, M. 2- and 4-nitrobenzenesulfonamides: exceptionally versatile means for preparation of secondary amines and protection of amines. *Tetrahedron Lett.* **1995**, *36*, 6373−6374.
(43) Maligres, P. E.; See, M. M.; Askin, D.; Reider, P. J. Nosylaziridines: activated aziridine electrophiles. *Tetrahedron Lett.* **1997**, *38*, 5253−5256.
(44) Mitsunobu, O. The use of diethyl azodicarboxylate and triphenylphosphine in synthesis and transformation of natural products. *Synthesis* **1981**, *1*, 1−28.
(45) Blanchette, M. A.; Choy, W.; Davis, J. T.; Essenfeld, A. P.; Masamune, S.; Roush, R. W.; Sakai, T. Horner-Wadsworth-Emmons reaction: Use of lithium chloride and an amine for base-sensitive compounds. *Tetrahedron Lett.* **1984**, *25*, 2183−2186.
(46) Abdel-Magid, A. F.; Maryanoff, C. A.; Carson, K. G. Reductive amination of aldehydes and ketones by using sodium triacetoxyborohydride. *Tetrahedron Lett.* **1990**, *31*, 5595−5598.
(47) Honzl, J.; Rudinger, J. Amino acids and peptides. XXXIII. Nitrosyl chloride and butyl nitrite as reagents in peptide synthesis by the azide method; suppression of amide formation. *Collect. Czech. Chem. Commun.* **1961**, *26*, 2333−2344.
(48) Nakashima, H.; Masuda, M.; Murakami, T.; Koyanagi, Y.; Matsumoto, A.; Fujii, N.; Yamamoto, N. Anti-human immunodeficiency virus activity of a novel synthetic peptide, T22 ([Tyr-5, 12, Lys-7]polyphemusin II): a possible inhibitor of virus-cell fusion. *Antimicrob. Agents Chemother.* **1992**, *36*, 1249−1255.
(49) Navenot, J. M.; Wang, Z. X.; Trent, J. O.; Murray, J. L.; Hu, Q. X.; DeLeeuw, L.; Moore, P. S.; Chang, Y.; Peiper, S. C. Molecular anatomy of CCR5 engagement by physiologic and viral chemokines and HIV-1 envelope glycoproteins: Differences in primary structural requirements for RANTES, MIP-1α, and vMIP-II binding. *J. Mol. Biol.* **2001**, *313*, 1181−1193.
(50) Intramolecular hydrogen bonds were not observed in the calculated structure. Thus, the EADI-containing pseudopeptides, which are discussed in this study, do not seem to exist in a characteristic turn conformation such as a βII′γ turn as reported in several papers concerning normal cyclic pentapeptides, see Nikiforovich, G. V.; Kover, K. E.; Zhang, W.-J.; Marshall, G. R. Cyclopentapeptides as flexible conformational templates. *J. Am. Chem. Soc.* **2000**, *122*, 3262−3273.
(51) Miyamoto, K.; Nakagawa, T.; Kuroda, Y. Solution structure of the cytoplasmic linker between domain III−S6 and domain IV−S1 (III−IV linker) of the rat brain sodium channel in SDS micelles. *Biopolymers* **2001**, *59*, 380−393.
(52) Ludvigsen, S.; Andersen, K. V.; Poulsen, F. M. Accurate measurements of coupling-constants from 2-dimensional nuclear-magnetic-resonance spectra of proteins and determination of φ-angles *J. Mol. Biol.* **1991**, *217*, 731−736.

JM049429H

THE JOURNAL OF BIOLOGICAL CHEMISTRY
Vol. 280, No. 11, Issue of March 18, pp. 9895–9903, 2005
Printed in U.S.A.

Bioluminescence Resonance Energy Transfer Reveals Ligand-induced Conformational Changes in CXCR4 Homo- and Heterodimers*

Received for publication, September 29, 2004, and in revised form, December 22, 2004
Published, JBC Papers in Press, January 4, 2005, DOI 10.1074/jbc.M411151200

Yann Percherancier‡§, Yamina A. Berchiche‡¶, Isabelle Slight‡¶, Rudolf Volkmer-Engert‖, Hirokazu Tamamura, Nobutaka Fujii**, Michel Bouvier‡§§, and Nikolaus Heveker‡¶‡‡**

*From the ‡Department of Biochemistry, Université de Montréal, Montréal H3C 3J7, Québéc, Canada, the ¶Research Centre/Hôpital Sainte-Justine, Montréal, Québec, H3T 1C5, Canada, the ‖Institute for Medical Immunology, Department of Molecular Libraries, Charité-Universitätsmedizin, 10117 Berlin, Germany, and **Graduate School of Pharmaceutical Sciences, Kyoto University, Kyoto 606-8501, Japan*

Homo- and heterodimerization have emerged as prominent features of G-protein-coupled receptors with possible impact on the regulation of their activity. Using a sensitive bioluminescence resonance energy transfer system, we investigated the formation of CXCR4 and CCR2 chemokine receptor dimers. We found that both receptors exist as constitutive homo- and heterodimers and that ligands induce conformational changes within the pre-formed dimers without promoting receptor dimer formation or disassembly. Ligands with different intrinsic efficacies yielded distinct bioluminescence resonance energy transfer modulations, indicating the stabilization of distinct receptor conformations. We also found that peptides derived from the transmembrane domains of CXCR4 inhibited activation of this receptor by blocking the ligand-induced conformational transitions of the dimer. Taken together, our data support a model in which chemokine receptor homo- and heterodimers form spontaneously and respond to ligand binding as units that undergo conformational changes involving both protomers even when only one of the two ligand binding sites is occupied.

In recent years, the concept of GPCR[1] dimerization has raised questions about the molecular details and functional role of such oligomeric assembly (for a recent review, see Ref. 1). Given the clinical interest in GPCRs, insights into the structural and functional organization of the receptor complexes have the potential to facilitate the design of new drug candidates with increased efficacy and selectivity. Resonance energy transfer (RET) techniques have emerged as methods of choice to study receptor dimerization in living cells. Although most RET studies indicate that many if not all GPCRs exist as dimers or higher oligomers under basal conditions, apparent contradictions exist concerning their potential dynamic regulation upon ligand binding. Although numerous authors did not find any effects of ligands on constitutive RET signals in their systems (2–8), others observed ligand-promoted increases or decreases that were interpreted as either the formation (9–11) or the dissociation (12–15) of GPCR dimers in response to receptor activation. Conformational changes within pre-existing constitutive dimers have also been proposed as alternative explanations for agonist or antagonist-induced changes in RET (16–18).

Chemokine receptors such as CCR2 and CXCR4 have been reported to form homo- and heterodimers (3, 4, 19–24). In early co-immunoprecipitation studies, Vila-Coro *et al.* (21) proposed that the dimerization of CXCR4 is induced upon activation by its chemokine ligand SDF-1. In contrast, data obtained with RET techniques revealed that CXCR4 homo-dimers form spontaneously in the absence of ligand (3, 4, 24). In one study, no significant effect of SDF-1 was observed on the constitutive energy transfer (4), whereas a small but reproducible increase was detected by others (24). As for CXCR4, agonist stimulation of CCR2 was found to promote the formation of dimers as revealed by chemical cross-linking followed by immunoprecipitation, suggesting that receptor dimerization and activation are interconnected processes (19). Heterodimerization between CXCR4 and CCR2 has initially been proposed to occur only in the case of a frequent genetic variant of CCR2, termed CCR2V64I, but not for the wild-type form of CCR2 (20). Given that CCR2V64I was associated with delayed AIDS progression (25–27), such a specific heterodimerization pattern could have important pathophysiological consequences. Indeed, it has been speculated that the AIDS-protective phenotype of the variant could be the result of its block of HIV entry via CXCR4 (20). In line with this proposition, the same authors proposed that the antiviral properties of a monoclonal anti-CCR2 antiantibody resulted from its ability to force the heterodimerization of CCR2 with CXCR4 (23).

Taken together, the results summarized above raise a number of questions concerning the dynamic nature of the homo- and heterodimerization processes regulating GPCR function.

* This work was supported in part by grants from the Canadian Institutes of Health Research (to N. H. and M. B.), the Canadian Foundation for Innovation, and the Fondation de l'Hôpital Sainte Justine. The costs of publication of this article were defrayed in part by the payment of page charges. This article must therefore be hereby marked "*advertisement*" in accordance with 18 U.S.C. Section 1734 solely to indicate this fact.

§ Supported by the Institut National de la Santé et de la Recherche Médicale (INSERM, France) and the Canadian Institutes of Health Research.

§§ Canada Research Chair in Signal Transduction and Molecular Pharmacology.

‡‡ Recipient of a scholarship from the Fonds de la Recherche en Santé du Québéc. To whom correspondence should be addressed: Centre de Recherche, 6737 Hôpital Sainte-Justine, 3175 Chemin de la Côte Sainte-Catherine, Montréal, Québec, H3T 1C5, Canada. Tel.: 514-345-4931 (ext. 4190); Fax: 514-345-4801; E-mail: nikolaus.heveker@recherche-ste-justine.qc.ca.

[1] The abbreviations used are: GPCR, G-protein-coupled receptor; RET, resonance energy transfer; BRET, bioluminescence resonance energy transfer; HEK, human embryonic kidney; PBS, phosphate-buffered saline; YFP, yellow fluorescent protein; RLuc, *Renillia* luciferase; BSA, bovine serum albumin; $BRET_{50}$, 50% of the maximal BRET signal; HIV, human immunodeficiency virus; TM, transmembrane.

Among these, the question of whether receptor ligands can induce homo- or heterodimer association or dissociation or promote conformational changes within preformed dimers that remain stable through the activation cycle is still highly debated. The potential role of CXCR4/CCR2 heterodimerization in inhibiting HIV entry makes it a particularly relevant model to study this question. In addition to their role in HIV infection, these chemokine receptors have been shown to be involved in cancer metastasis as well as in various aspects of inflammatory diseases including the directed migration of leukocytes during acute immune responses and homing (28–34). Therefore, understanding the dynamics of CXCR4/CCR2 homo- and heterodimerization after ligand binding takes on a particular importance when considering their potential as drug targets for numerous disease states.

In the present study, we took advantage of bioluminescence resonance energy transfer (BRET) approaches to study CXCR4/CCR2 homo- and heterodimers in the course of receptor activation. We found that CXCR4 and CCR2 exist as constitutive homo- and heterodimers and that different ligands promote distinct conformational rearrangements of preformed stable oligomers. Our data also indicate that peptides derived from CXCR4 transmembrane domains block receptor activation by preventing the agonist-promoted conformational rearrangement of both CXCR4 homo- and CXCR4/CCR2 heterodimers.

EXPERIMENTAL PROCEDURES

Plasmids—The cloning of CXCR4-YFP and CXCR4-RLuc have been described previously (3). CCR2-YFP and CCR2-RLuc were constructed by ligating the coding sequence of CCR2, after its amplification by PCR, into the pGFP-N1-Topaze (PerkinElmer Life and Analytical Sciences) and (hRLuc)-N3 (BioSignal) backbones of the CXCR4-YFP and -RLuc using the HinDIII and AgeI or HinDIII and BamHI sites, respectively. The constructs were sequenced to ensure the absence of unwanted mutations. The 64V and 64I variants were obtained by site-directed mutagenesis using the Kunkel method. The amino acid sequence of the fusion linker regions between the terminal receptor residue and the initiator methionine of either YFP or RLuc were as follows: CXCR4-YFP, FHSS***KPVAT***MVSKG; CXCR4-RLuc, FHSS***KPGDPPARAT***-MTSKV; CCR2-YFP, SAGL***GPVAT***MVSKG; and CCR2-RLuc, SAGL-***GDPPARAT***MTSKV. Bold italic characters identify linker residues resulting from the cloning strategy and that derive neither from the receptor nor the fluorophore sequences. The sequences of the linker regions and of the mutated residues were verified by direct sequencing.

Reagents—SDF-1 and MCP-1 were purchased from PeproTech and AMD3100 was obtained from the NIH AIDS Research & Reference Reagent Program. TC14012, a T140 analogue with similar biological properties, was synthesized as described previously (35). The sequences of the CXCR4 transmembrane domain-derived peptides as described in Tarasova *et al.* (36) were synthesized using Fmoc (*N*-(9-fluorenyl)methoxycarbonyl) solid phase synthesis as described previously (37), purified to >95% purity and characterized by matrix-assisted laser desorption ionization/time of flight mass spectrometry. The sequences of the peptides are as follows: CXCR4-TMII, LLFVITLPFWAVDAVANWYFGN-DD-OH; CXCR4-TMIV, VYVGVWIPALLLTIPDFIFANDD-OH; CXCR-4-TMVI, VILILAFFACWLPYYIGISID-OH; CXCR4-TMVII, DDEALA-FFHCCLNPILYAFL-NH_2. β2AR-TMVI-1 (NH_2-GIIMGTFTLCWLPFF-IVNIVH-COOH) and β2AR-TMVI-2 (NH_2-AIIMATFTACWLPFFIVNI-VH-COOH) were described in Ref. 38. They were dissolved as 10 mM stocks in Me_2SO and used freshly diluted at the concentrations indicated in the text and in the figure legends.

Cell Culture and Transfection—HEK293T cells were maintained in Dulbecco's modified Eagle's medium supplemented with 10% fetal bovine serum, 100 units/ml penicillin and streptomycin, 2 mM L-glutamine (all from Wisent). 24 h before transfection, cells were seeded at a density of 500,000 cells per well in 6-well dishes. Transient transfections were performed using the FuGENE-6 transfection reagent (Roche) in OptiMEM medium (Invitrogen) In general, 0.1 μg of CXCR4-RLuc or CCR2-RLuc was transfected alone or with increasing quantities of YFP-tagged CXCR4 or CCR2. The total amount of DNA transfected in each well was completed to 2 μg with empty vector. After overnight incubation, transfection medium was replaced with fresh Dulbecco's modified Eagle's medium for 3 h to allow cell recovery. Transfected cells were then seeded in 96-well white plates (with clear bottoms that had been pre-treated with poly-D-lysine) and left in culture for 24 h before being processed for BRET assay.

Flow Cytometry—Transfected HEK293T cells were detached with phosphate-buffered saline (PBS) containing 1 mM EDTA 24 h after cotransfection with CXCR4-RLUC and CXCR4-YFP as indicated. Peripheral blood mononuclear cells (PBMC) were isolated on a Ficoll (Amersham Biosciences) gradient from whole blood. The cells were stimulated with 10 μg/ml phytohemagglutinin and cultured for 7 days in RPMI containing 10% fetal bovine serum and 50 IU/ml interleukin-2. For CXCR4 staining, the cells were incubated 45 min at 4 °C in PBS containing 2% fetal bovine serum with anti-CXCR4 phycoerythrin-conjugated 12G5 monoclonal antibody (Santa Cruz Biotechnology). They were then washed three times with PBS, and cell surface expression of CXCR4 was quantified by flow cytometry on a FACSCalibur flow cytometer (BD Biosciences).

BRET Assays—For routine BRET measurements, cells were washed once with PBS 36 to 48 h after transfection and coelenterazine H (Nanolight Technology) added to a final concentration of 5 μM in PBS. Readings were then collected using a multidetector plate reader MITHRAS LB940 (Berthold Technologies, Bad Wildbad, Germany) allowing the sequential integration of the signals detected in the 480 ± 20 nm and 530 ± 20 nm windows for luciferase and YFP light emissions respectively. The BRET signal is determined by calculating the ratio of the light intensity emitted by the Receptor-YFP over the light intensity emitted by the Receptor-RLuc. The values were corrected by subtracting the background BRET signal detected when the Receptor-RLuc construct was expressed alone. To assess the effects of ligands, SDF-1, AMD3100, TC14012, and MCP-1 were added at the concentrations indicated in the text and in the figure legends and incubated at 37 °C for 5 min before the addition of coelenterazine H and BRET reading. When indicated, ligands were added in presence of 0.1% BSA (Sigma). For experiments with transmembrane peptides, the cells were pre-incubated with the different peptides in PBS for 15 min at 37 °C before agonist exposure.

For acquisition of full BRET spectra, cells were transfected as described above with different amounts of CXCR4-YFP for a given quantity of CXCR4-RLuc (0.1 μg). Cells were detached and resuspended in PBS containing 0.1% (w/v) glucose. 200,000 cells were seeded in 100 μl of PBS in a 96-well plate with a clear bottom (Corning), and BRET scan was performed in a Flex-station 2 (Molecular Devices) by reading luminescence between 400 and 600 nm immediately after the addition of coelenterazine for cells expressing different [acceptor]/[donor] ratios.

For BRET titration experiments, net BRET ratios were expressed as a function of the [acceptor]/[donor] ratio (39). Total fluorescence and luminescence were used as relative measures of total expression of the acceptor and donor proteins, respectively. Total fluorescence was determined with MITHRAS using an excitation filter at 485 nm and an emission filter at 535 nm. Total luminescence was measured in the MITHRAS, 10 min after the addition of coelenterazine and the reading taken in the absence of emission filter.

cAMP Production—To determine cAMP accumulation, HEK293T cells were seeded in 24-well microplates at 10^5 cells/well (coated with 0.1% poly-D-lysine) 24 h before the experiment and labeled for 2–3 h in Dulbecco's modified Eagle's medium without fetal bovine serum containing 2 μCi/ml [^{3}H]adenine (PerkinElmer Life and Analytical Sciences). Because CXCR4 is coupled to Gi proteins, the relative efficacy of SDF-1 to inhibit forskolin-induced cAMP production was monitored in different conditions. Cells were stimulated in presence of 20 μM forskolin (Sigma) alone or 20 μM forskolin and 1 nM SDF-1 for 30 min at 37 °C in Dulbecco's modified Eagle's medium containing 50 mM HEPES, pH 7.4, 0.1% BSA, 1 mM 3-isobutyl-1-methylxanthine (Sigma) and supplemented or not with 10 μM of each of the CXCR4 TM peptides. The reaction was terminated by removing the Dulbecco's modified Eagle's medium/3-isobutyl-1-methylxanthine/ligand solution and the addition of ice-cold 5% trichloroacetic acid. [^{3}H]cAMP was purified by sequential chromatography (Dowex resin/aluminum oxide).

Binding Assays—SDF-1 binding to CXCR4 was assessed indirectly by flow cytometry as described previously (40). In brief, the ability of SDF-1 to compete for the binding of the monoclonal anti-CXCR4 antibody 12G5 to CEM cells was used to determine SDF-1 binding. SDF-1 was co-incubated at 4 °C for 30 min with the antibody and SDF binding determined by the loss of 12G5 labeling, as determined by flow cytometry. To test whether CXCR4 TM peptides interfered with SDF-1 binding to CXCR4, the peptides were incubated with the cells 15 min before addition of SDF-1 and 12G5. Control tubes were incubated with peptides and 12G5, without SDF-1.

For T14012 binding assay, CXCR4-expressing HEK293T cells were detached with 5 mM EDTA, washed twice in binding buffer (50 mmol/L

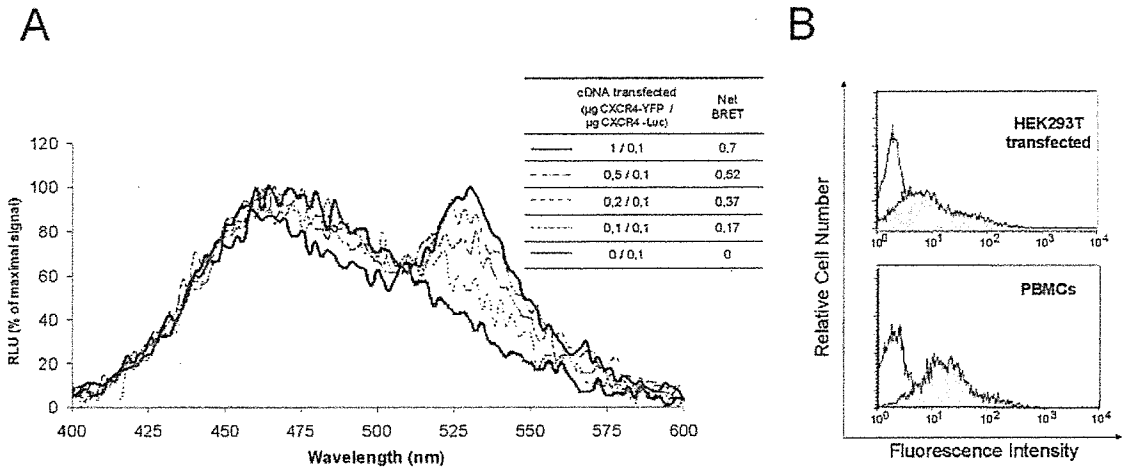

FIG. 1. *A*, light emission BRET spectra for CXCR4 homodimerization. Spectra of HEK293T cells coexpressing a fix amount of BRET donor (CXCR4-RLuc) and various levels of acceptor (CXCR4-YFP). Net BRET signals and BRET spectra were determined in parallel. Results are expressed as percentage of the maximum signal obtained when CXCR4-RLuc is transfected alone. *B*, CXCR4 expression of transfected and primary cells: relative CXCR4 expression in transiently transfected HEK293T cells (0.1 μg of CXCR4-Luc and 1 μg of CXCR4-YFP) and in activated peripheral mononuclear blood cells (*PBMCs*) by flow cytometry using the anti-CXCR4-PE antibody.

HEPES, pH 7.4, 1 mmol/L $CaCl_2$, 5 mmol/L $MgCl_2$, and 0.5% BSA) and resuspended at final concentration of 5×10^5 cells/ml. Total SDF-1 binding was measured with 0.1 nM ^{125}I-SDF-1 (2200 Ci/mmol; PerkinElmer Life and Analytical Sciences) as tracer, and TC14012 competition assays were performed with 100 nM TC14012 in the presence or absence of 10 μM of each CXCR4 peptide. The samples were incubated for 90 min at 20 °C, and binding was terminated by rapid filtration through glass fiber (GF/C) filters (Whatman) using ice-cold PBS containing 0.5 M NaCl. The retained radioactivity was counted in a γ counter (1271 RIAgamma Counter; PerkinElmer Life and Analytical Sciences).

Data Analysis—Data obtained in BRET assays were analyzed using Prism 3.0. Statistical significance of the differences between the different conditions were calculated using one-way analysis of variance with a Bonferroni post-test for p values less than 0.05.

RESULTS

Constitutive CXCR4 Dimers Revealed by BRET—The existence of constitutive CXCR4 dimers was probed by monitoring the occurrence of intermolecular interactions among CXCR4 molecules under basal conditions using a proximity-based BRET assay. For this purpose, a constant amount of CXCR4-RLuc expression vector was cotransfected with increasing amounts of CXCR4-YFP encoding plasmid. The entire emission spectrum between 400 and 600 nm was then analyzed for various CXCR4-YFP/CXCR4-RLuc (energy acceptor/energy donor) ratios after the addition of the luciferase substrate coelenterazine. As shown in Fig. 1, increasing the expression level of CXCR4-YFP led to a progressive increase in the amount of light emitted in the 510–550 nm region that resulted from the transfer of energy from the luciferase to the YFP with the ensuing emission of light by the latter (Fig. 1*A*). The occurrence of BRET between RLuc and YFP was further illustrated by the reduction in emission observed in the 450–510 nm part of the spectrum that corresponds to the region of overlap between RLuc (energy donor) emission and YFP (energy acceptor) excitation wavelengths allowing the energy transfer. The basal BRET observed in the absence of any receptor ligand indicates, in agreement with previous reports (3, 4, 24), that CXCR4 exists as a constitutive homodimer. For all subsequent BRET experiments, the emission of light was measured only in the 460–500 nm and 510–550 nm windows, corresponding to the RLuc and YFP emission peaks, respectively, and the BRET defined as the ratio of light detected in these two channels after coelenterazine addition. As can be seen in Fig. 2*A*, the BRET signal increased as a hyperbolic function of the CXCR4-YFP/CXCR4-RLuc ratio. The saturation of the BRET titration curve is indicative of a specific protein-protein interaction, because random molecular collisions that would give rise to bystander BRET would be expected to increase nearly linearly over a wide range of YFP/RLuc (39, 41). The selectivity of the observed signal is further supported by the fact that co-expression of CXCR4-RLuc with an unrelated GPCR, GBR2-YFP, led to marginal signal that progressed linearly over the same range of energy acceptor/donor. The positive BRET signal did not result from a non-physiological overexpression of the receptors, because CXCR4 immunostaining followed by flow cytometry analysis revealed that the highest expression levels reached in transfected HEK293T cells (1 μg of CXCR4-YFP + 0.1 μg of CXCR4-RLuc) was still lower than those observed in activated peripheral blood mononuclear cells (Fig. 1*B*).

Ligand-induced Modulation of the CXCR4 Homodimer BRET Signal—To assess the effect of ligand binding on the BRET signal observed for the CXCR4 homodimer, full BRET titration curves were obtained in the presence and absence of the CXCR4 agonist SDF-1 or the polyphemusin II-derived inverse agonists peptide analogue TC14012 (35). As can be seen in Fig. 2*A*, the addition of SDF-1 increased the maximal BRET signal observed, whereas TC14012 decreased it. It is interesting that neither compound affected the shape of the curve so that the concentration of CXCR4-YFP needed to reach 50% of the maximal BRET signal ($BRET_{50}$) remained unaffected by the treatments. Because the $BRET_{50}$ represents the propensity of the protomers to interact with one another (*i.e.* their relative affinity), our data indicate that the ligand treatments did not change the number of complexes. Rather, the maximal BRET signal increase most likely reflects conformational changes, within preformed receptor dimers, that affect the distance between the energy donor and acceptor. SDF-1 had no effect on the marginal signal observed between CXCR4-RLuc and the unrelated GBR2-YFP, confirming the selectivity of the effect.

The dose dependence of the ligand effect is illustrated in Fig. 2*B*. In cell expressing a given CXCR4-RLuc/CXCR4-YFP ratio, the agonist SDF-1 and inverse agonist TC14012 dose-dependently increase and decrease the basal BRET signal, respectively. It is interesting that the bicyclam weak partial agonist AMD3100 (42) increases the BRET signal, albeit to lower extent than the full agonist SDF-1. The unrelated CCR2-selective chemokine MCP-1 had no effect on the BRET signal, confirming that ligand interaction with CXCR4 is required to promote BRET changes. The dose-response curves were carried out in

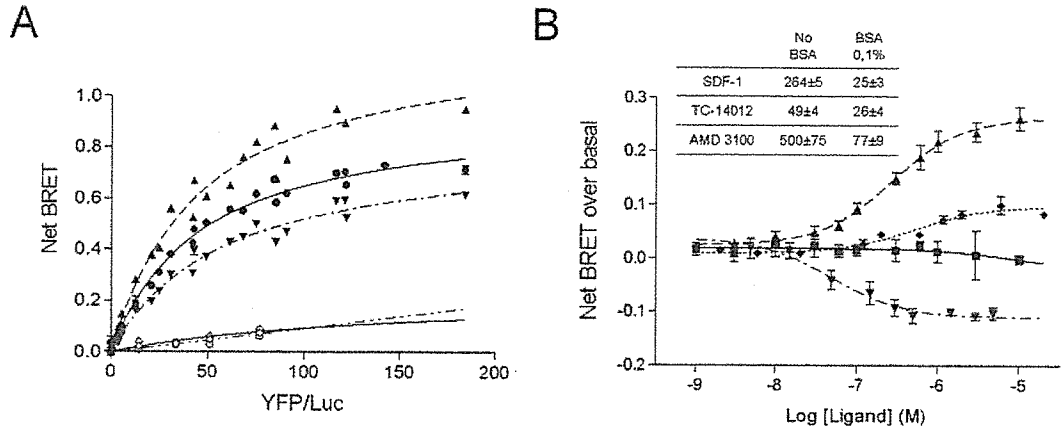

FIG. 2. **Ligand effect on CXCR4 homodimers expressed at physiological levels in HEK293T cells.** HEK293T cells were transiently transfected with 0.1 μg of CXCR4-RLuc and different amounts ranging from 0.03 to 1 μg (*A*) or 1 μg (*B*) of CXCR4-YFP. *A*, saturation curves with and without ligands (700 nM SDF-1 or 500 nM TC14012). Saturation curves were obtained by plotting net BRET as a function of the [Acceptor]/[Donor] ratio (for more detail, see "Experimental Procedures"). As a control of specificity, CXCR4-RLuc BRET was also monitored with increasing quantities of GBR2-YFP in presence (○) or absence (◇) of 700 nM SDF-1. Result represents one experiment of five that gave similar results. $BRET_{50}$ values, measured without ligand or in the presence of SDF-1 or TC14012, were 45.8 ± 3, 46 ± 4.7, and 57.2 ± 5.2, respectively. *B*, dose-response of ligand-induced change in CXCR4/CXCR4 homodimerization BRET. 48 h after transfections, cells were activated for 5 min at 37 °C with increasing concentration of SDF-1, AMD3100, MCP-1, or TC14012 before BRET measurement. The inset compares the nanomolar EC_{50} values found for SDF-1, TC14012, and AMD3100 in the presence or absence of 0.1% BSA used as carrier protein. The results represent the average ± S.E. of four independent experiments done in duplicate. ▲, SDF-1; ▼, TC14012; ♦, AMD3100; ■, MCP-1; ●, no ligand.

both the absence and the presence of the carrier protein BSA (0.1%). As can be seen in the Table inset, the presence of BSA significantly increased the apparent potency of the compounds, indicating the occurrence of nonspecific adsorption or inactivation of the diluted ligands in the absence of carrier. The EC_{50} determined for SDF-1 in the presence of BSA was well within the range of K_d values previously reported for SDF-1 binding to CXCR4 (4–85 nM) (43–47), whereas the EC_{50} for TC14012 and AMD3100 are comparable with the IC_{50} values obtained in binding competition experiments using ^{125}I-SDF-1 as the radioligand (42).

The pharmacological selectivity of the ligand-promoted BRET changes was further demonstrated by the competitive nature of the effects. Indeed, as shown in Fig. 3, TC14012 dose-dependently blocked the ability of 100 nM SDF-1 to increase the BRET signal and eventually reverse this increase revealing the inhibitory action of the inverse agonist (Fig. 3*A*). Likewise, increasing concentration of the partial agonist AMD3100 progressively blocked the SDF-1-promoted BRET increase until it reached the modestly elevated level corresponding to the partial agonistic activity of AMD3100 (Fig. 3*B*). Taken together, these results indicate that three compounds with different intrinsic efficacies led to distinct conformational changes of the CXCR4 dimer.

CCR2 Homo- and Heterodimers—CXCR4 has been previously demonstrated to form heterodimers with CCR2, but it remained unclear whether these heterodimers are spontaneously formed or induced by the presence of one or both receptor ligands (20, 23, 48). To clarify this issue, we first investigated the formation of constitutive CCR2 homodimers and their modulation by the CCR2 selective agonist MCP-1. As can be seen in Fig. 4*A*, saturating hyperbolic BRET titration curves revealed the spontaneous formation of CCR2 homodimer. The selective agonist increased the maximal BRET signal without affecting the $BRET_{50}$ in a manner similar to that observed for the constitutive CXCR4 homodimer, indicating that the conformation and not the number of dimers was affected by the ligand binding. The pharmacological selectivity of the effects was again confirmed by the fact that the CXCR4-selective agonist SDF-1 had no effect on the CCR2 dimer BRET signal (Fig. 4*B*).

As was the case for each of the receptors expressed individually, coexpression of CCR2 and CXCR4 led to the formation of constitutive heterodimers revealed by specific basal BRET signals and hyperbolic saturating BRET titration curves between CCR2-RLuc and CXCR4-YFP as well as in the reverse orientation (between CXCR4-RLuc and CCR2-YFP) (Fig. 5*A*). It is interesting that the selective binding of ligands to a single protomer was sufficient to promote heterodimer BRET changes for the two BRET orientations. However, the pattern of ligand effects was different from that observed for each of the homodimers. In addition, the BRET pair orientation influenced the ligand response pattern. When considering the CXCR4-RLuc/CCR2-YFP orientation, the addition of the CCR2 agonist MCP-1 led, as was the case for the CCR2 homodimer, to an increase of the heterodimer BRET signal. In contrast, the CXCR4 agonist SDF-1, which promoted an increase of the CXCR4 homodimer BRET, decreased the BRET signal originating from the heterodimer. The CXCR4 inverse agonist TC14012 for its part had a similar effect on the homo- and heterodimer, leading to a decrease in the BRET signal (Fig. 5*B*, *left*). When the reverse BRET partner orientation (CCR2-RLuc/CXCR4-YFP) was investigated, the CXCR4 ligands SDF-1 and TC14012 retained their inhibitory effect on the heterodimer BRET signal. MCP-1, however, which increased the BRET observed between CXCR4-RLuc and CCR2-YFP, led to a dramatic reduction of the BRET signal obtained for the CCR2-RLuc/CXCR4-YFP pair (Fig. 5*B*, *right*). Taken together, these results clearly indicate that the orientation of the ligand-promoted BRET changes cannot be used as a direct reflection of the intrinsic ligand efficacy. Rather, it seems to be dependent on both the nature of the ligand and the BRET pairs considered; both the identity of the receptor protomers and the relative position of the energy donor and acceptor within the dimers influence the responses observed.

The observation that MCP-1 can either increase or decrease the BRET signal emanating from the CXCR4/CCR2 heterodimer depending on the relative RLuc/YFP orientation can hardly be reconciled with the hypothesis that BRET changes reflect ligand-induced dimer association or dissociation. Indeed, the same ligand should not lead to opposite effects on the same receptor heterodimer. Given that both the distance and the orientation between the energy donor and acceptor determine the BRET efficacy, the distinct BRET modulations observed most probably reflect conformational rearrangements

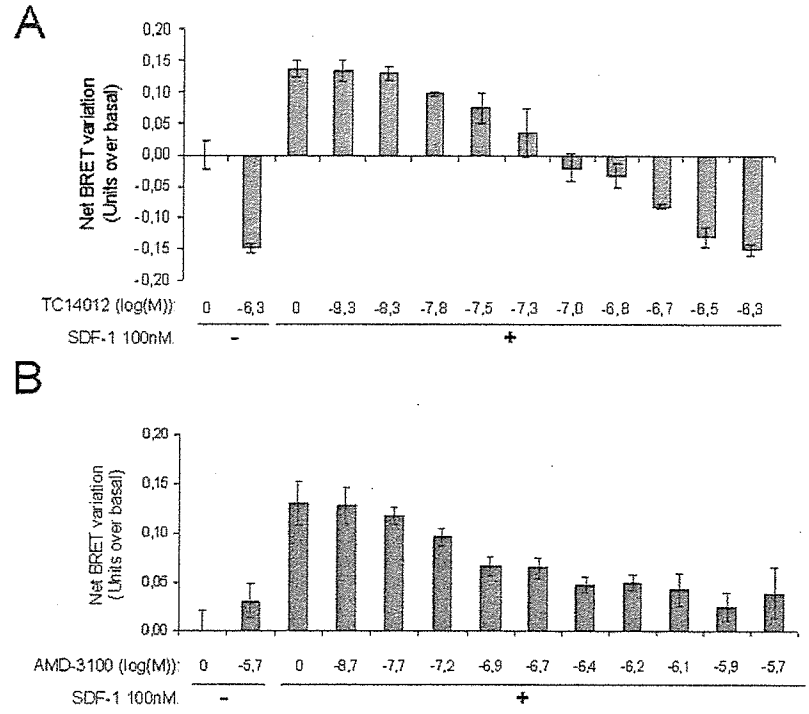

FIG. 3. **TC14012 and AMD3100 competition of SDF-1α induced changes in CXCR4 homodimerization BRET signal.** HEK293T cells were transfected with 0.1 μg of CXCR4-RLuc and a saturating quantity (1.0 μg) of CXCR4-YFP plasmids. Ligands were added either alone (100 nM SDF-1, 500 nM TC14012, or 2 μM AMD3100), or 100 nM SDF-1 was mixed with increasing quantities of TC14012 or AMD3100. Results are the average of three independent experiments performed in duplicate.

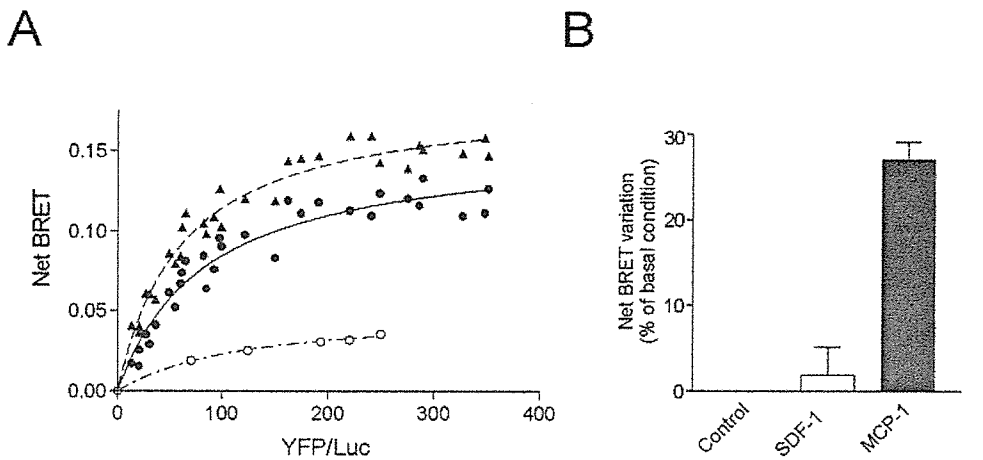

FIG. 4. **MCP-1 effect on CCR2 homodimers.** *A*, HEK293T cells were transfected with 0.1 μg of CCR2-RLuc and increasing quantities (from 0.01 to 1.0 μg) of either CCR2-YFP (●, ▲) or GBR2-YFP (○) vectors. Net BRET measured in presence (▲) or absence (●, ○) of 200 nM MCP-1 is plotted as a function of the [Acceptor]/[Donor] ratio as in Fig. 2. $BRET_{50}$ values measured for CCR2 homodimer in absence and presence of MCP-1 were 84.2 ± 11.1 and 61.8 ± 5.8, respectively. *B*, cells transfected with 0.1 μg of CCR2-RLuc and a saturating excess (1.0 μg) of CCR2-YFP plasmids were stimulated with 200 nM MCP-1 or 200 nM SDF-1. Results are the average of three independent experiments performed in triplicate.

that change either the distance or the relative orientation between the fluorophores. Because these parameters are affected by the initial relative position of the RLuc and YFP within the dimers, it is to be expected that the same conformational switch imposed by a ligand could result in very different BRET changes when different BRET configurations are considered.

A previous study suggested that CXCR4/CCR2 heterodimers could be formed only with the CCR2V64I variant form of the receptor and not with the wild-type CCR2 (20). Given that the CCR2 64I variant is associated with delayed AIDS onset in persons infected with HIV, the finding was suggestive that the phenotype of the 64I variant could be mediated by an inhibition of CXCR4 usage by HIV as a result of its heterodimerization (23, 26). To reassess this possibility, we systematically used both CCR2 variants to measure both basal and ligand-modulated BRET signals generated by homo- and heterodimers but failed to detect any significant difference between them (data not shown). Therefore, the mechanism for the observed protective phenotype against AIDS progression of CCR2V64I is not related to its ability to heterodimerize with CXCR4.

Effects of Peptides Derived from the CXCR4 Transmembrane Domains on both CXCR4 Homo- and Heterodimers—Previous work had found that peptides derived from CXCR4 transmembrane domains are rapidly associating with the receptor, blocking its signaling as well as its HIV-1 coreceptor function (36). We asked whether these effects could result from the dissociation of constitutive CXCR4 dimers, a mechanism that had been suggested for the effect of a peptide derived from TMVI of the β-adrenergic receptor (38). For this purpose, the effect of four peptides derived from TMs II, IV, VI and VII was assessed on the basal CXCR4 homodimer BRET signal. As shown in Fig. 6*A*, none of the peptides affected the constitutive BRET signal as shown by the unaltered BRET titration curves, ruling out peptide-promoted dissociation as the basis of their functional inhibitory action. However, all peptides blocked the SDF-1-

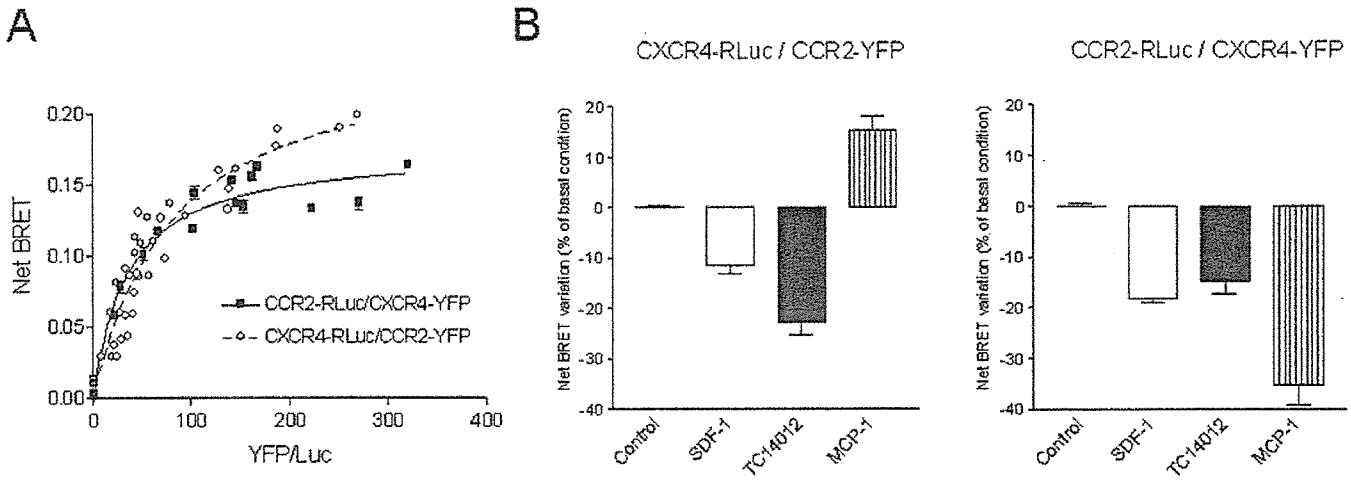

FIG. 5. **SDF-1, TC14012, and MCP-1 effects on CXCR4-CCR2 heterodimers.** HEK293T cells were transfected with 0.1 μg of either CXCR4-RLuc or CCR2-RLuc and different amounts ranging from 0.03 to 1.0 μg (*A*) or saturating excess (1.0 μg) (*B*) of CCR2-YFP or CXCR4-YFP expression vectors. *A*, CCR2-RLuc/CXCR4-YFP and CXCR4-RLuc/CCR2-YFP saturation curves were obtained by plotting net BRET as a function of the [acceptor]/[donor] ratio as explained in material and methods. *B*, HEK293T cells transfected either with CXCR4-RLuc/CCR2-YFP (*left*) or CCR2-RLuc/CXCR4-YFP (*right*) were stimulated with either 200 nM SDF-1α, 500 nM TC14012, or 200 nM MCP-1 for 5 min at 37 °C before BRET measurement.

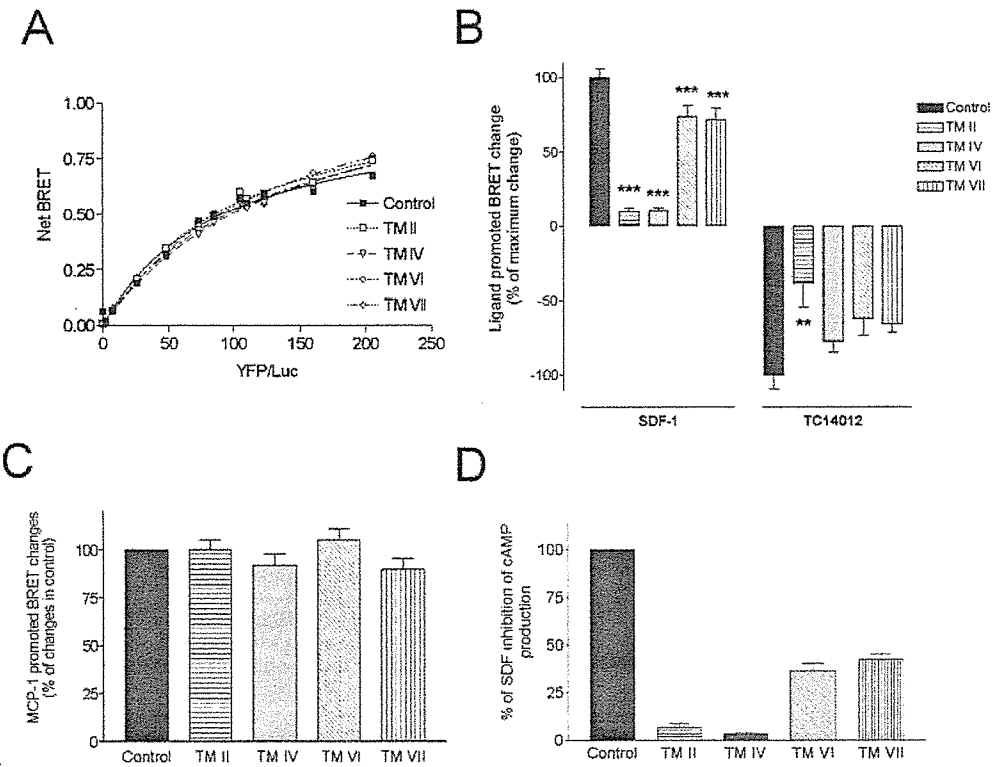

FIG. 6. **Effects of CXCR4 TM peptides on CXCR4 homodimers.** *A*, saturation curve of CXCR4 homodimers in the presence or absence of CXCR4 TM peptides. Transiently transfected cells were incubated for 15 min at 37 °C in presence or absence of 10 μM of CXCR4 TMs 2, 4, 6, or 7 before BRET measurement. Longer peptide incubation times (1 h to overnight) yielded identical results (data not shown). *B*, cells transfected with 0.1 μg of CXCR4-RLuc and saturating excess (1.0 μg) of CXCR4-YFP were incubated with 10 μM of CXCR4 TMII, TMIV, TMVI, or TMVII as in *A* before being stimulated with 200 nM SDF-1 or 100 nM TC14012. Asterisks indicate significance of the difference between the TM-treated condition and control condition (vehicle alone, *black bar*). ***, $p < 0.001$; **, $p < 0.01$. Absence of asterisk indicates $p > 0.05$. *C*, cells transfected with 0.1 μg of CCR2-RLuc and saturating excess (1.0 μg) of CCR2-YFP were left untreated or were treated with 10 μM concentrations of each CXCR4 TM peptide, as in *B*, but were activated with 200 nM MCP-1. *D*, HEK293T cells transfected with CXCR4-Luc and CXCR4-YFP were stimulated for 30 min at 37 °C with 20 μM forskolin alone or 20 μM forskolin plus 1 nM SDF-1 in the presence of the vehicle (control) or 10 μM of each CXCR4 TM peptide. The cAMP production was assessed by measuring the accumulation of [^{3}H]cAMP in cells pre-labeled with [^{3}H]adenine and expressed as percentage of the maximal SDF-mediated inhibition in the absence of peptide. Results are expressed as the mean ± S.E. of three to five independent experiments carried out in triplicate.

induced BRET increase, and TMs II and IV were the most efficacious (Fig. 6*B*), indicating that inhibition of the agonist-promoted conformational change could underlie the mechanism of action of the peptides. It is interesting that the efficacies of the peptides in the BRET assay were similar their relative ability to block SDF-1 promoted inhibition of adenylyl cyclase activity (Fig. 6*D*). Indeed, whereas TMs II and IV acted as complete inhibitors in both assays, TMs VI and VII acted as partial blockers at 10 μM. When considering the inverse-agonist TC14012, only TMII significantly attenuated the ligand-

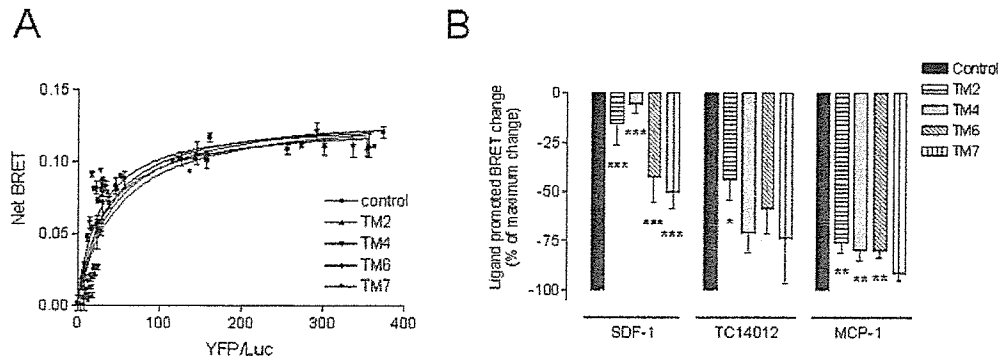

FIG. 7. **Effects of CXCR4 TM peptides on CCR2-CXCR4 heterodimers.** *A*, saturation curve of CCR2-CXCR4 heterodimers in the presence and absence of CXCR4 TM peptides. HEK293T cells transfected with 0.1 μg of CCR2-Luc and increasing quantities of CXCR4-YFP were incubated for 15 min at 37 °C in presence or absence of 10 μM of CXCR4 TMII, TMIV, TMVI, or TMVII before BRET measurement. *B*, HEK293T cells transfected with 0.1 μg of CCR2-RLuc and a saturating excess (1.0 μg) of CXCR4-YFP were treated with 10 μM of each CXCR4 TM peptide and stimulated with either 200 nM SDF-1, 100 nM TC14012, or 200 nM MCP-1. Results are expressed as the mean ± S.E. of five independent experiments carried out in triplicate. Asterisks indicate statistical significance of the difference between the TM-treated condition and control condition (vehicle alone, *black bar*) with ***, $p < 0.001$; **, $p < 0.01$; *, $p < 0.05$. Absence of asterisk indicates $p > 0.05$.

promoted BRET reduction; TMs IV, VI, and VII led only to marginal inhibition that did not reach statistical significance (Fig. 6*B*). The inhibitory action of the peptides seems to be directly linked to the inhibition of the activation process and not to the ligand binding to the receptor, because neither SDF-1 nor TC14012 binding to CXCR4 was affected by the peptides (data not shown). The differential effect of the peptides on the agonist- and inverse agonist-promoted changes further confirmed that the two ligands promoted distinct conformational changes that are differentially affected by the peptides. The effect was specific for CXCR4 because the peptides did not interfere with the MCP-1-induced increase of the CCR2 homodimer BRET signal (Fig. 6*C*). In addition, two peptides derived from the β2-adrenergic receptor TM VI (38) were without effect on the SDF-1 promoted increase in BRET between CXCR4-RLuc and CXCR4-YFP (data not shown).

We then examined the effect of the CXCR4-derived peptides on the CXCR4/CCR2 heterodimer. In the absence of ligands, the four peptides had no effect on the basal heterodimer BRET signal obtained between CCR2-RLuc and CXCR4-YFP (Fig. 7*A*), similar to what was observed for the CXCR4 homodimer. However, all four peptides blocked, albeit to different extents, the SDF-1-promoted BRET change, although only TMII significantly affected the TC14012-induced BRET reduction (Fig. 7*B*). This pattern of inhibition, which is similar to that observed for the CXCR4 homodimer suggests that comparable CXCR4 conformational changes occur upon ligand binding whether the receptor is part of an homodimer or within a CXCR4/CCR2 heterodimer. It is interesting that a modest (~25%) but statistically significant reduction of the heterodimer BRET response to the CCR2-selective agonist MCP-1 was also observed upon treatment with the CXCR4-derived TMII, TMIV, and TMVI peptides (Fig. 7*B*). This observation suggests that the heterodimer conformational changes induced by ligand binding to a single receptor protomer may not only involve changes within the ligand-bound receptor. Instead, trans-receptor conformational reorganization may be transmitted to the CXCR4 protomer upon ligand binding to the CCR2 protomer, and these transmitted conformational changes could be blocked by the CXCR4-derived peptides. On the other hand, the observed effects may be related to the capacity of the CXCR4-bound peptides to reduce CCR2 movements within the heterodimer.

DISCUSSION

Recent appreciation that GPCRs exist as dimers has raised a number of questions regarding the molecular dynamics and functional role of such oligomeric organization. Among these, whether dimerization is a constitutive phenomenon or is promoted by ligand binding remains highly debated. The role of dimerization in the receptor activation process also remains poorly understood. In this article, we present evidence indicating that, at least for CXCR4 and CCR2, receptors exist as constitutive homo- and heterodimers and that ligand binding induces conformational changes within pre-existing complexes without promoting the formation or dissociation of dimers. Taking advantage of CXCR4-derived peptides that can noncompetitively block receptor function, we also showed that ligand promoted changes in dimer conformations are intimately linked with receptor function.

Previous studies have led to conflicting interpretations concerning the dynamic nature of GPCR dimers. In particular, although many authors interpreted ligand-promoted changes in resonance energy transfer signals between GPCR protomers as evidence for receptor dimer formation or dissociation, (9, 12–14, 48), others inferred conformational changes within constitutive receptor dimers (16, 17, 41).

When considering CXCR4 and CCR2, early co-immunoprecipitation studies suggested that dimers formed only after stimulation with chemokines (20–22). Later work using either fluorescence or bioluminescence resonance energy transfer methods revealed the existence of spontaneous CXCR4 dimers (3, 4, 24). In two of these studies, the effect of the agonist SDF-1- was assessed on the basal RET signals. Whereas a modest increase that did not reach statistical significance was observed in one study (4), a reproducible increase was observed in the other (24). However, the data obtained did not allow determination of whether the RET augmentation represented an increase in dimer formation or a conformational change within the preformed dimers.

In the present study, in addition to confirming the existence of constitutive CXCR4 homodimers, our BRET results demonstrate that both CCR2 homodimers and CXCR4/CCR2 heterodimers can form spontaneously. Three lines of evidence supported that the basal BRET signals observed truly represent specific constitutive dimerization and are not simply nonspecific "bystander BRET" that would result from tight random-packing of monomeric receptors: 1) BRET titration experiments gave rise to saturating hyperbolic curves that are characteristic of specific protein-protein interactions rather than random molecular collisions (39), 2) no specific BRET signal could be detected between either CXCR4 or CCR2 and the unrelated GABAbR2, 3) receptor occupancy resulted in

either ligand-specific increases or decreases of the BRET signal; such a result would not be expected if the basal BRET signal resulted from nonspecific random collisions. In addition, the receptor expression levels of the transfected cells used in this study are similar to those observed in primary lymphocytes, thereby excluding the idea that dimerization is a result of receptor overexpression.

Our study also provides a conclusive demonstration that ligand-promoted modulation of CXCR4 and CCR2 homo- and heterodimer BRET signals results not from changes in dimer numbers but from the rearrangements of preformed dimers. First, the BRET titration curves revealed that the $BRET_{50}$ values, which would be expected to change if the propensity to form dimers was affected (39, 49), were unaltered in the presence of an agonist or an inverse agonist, suggesting that the ligands did not affect the apparent affinity of the receptor protomers for one another. Changes in maximal BRET signal in the absence of apparent altered affinity is best explained by conformational changes that change the distance and/or orientation between the energy donor and acceptor affecting the energy transfer efficacy. Second, the dependence of the MCP-1-promoted change in BRET signal on the orientation of the CXCR4/CCR2 heterodimer BRET partners (*i.e.* MCP-1 increased the BRET signal for the CXCR4-RLuc/CCR2-YFP pair but decreased it for CCR2-RLuc/CXCR4-YFP) is hardly compatible with ligand-promoted dimer formation or dissociation. In fact, it seems highly unlikely that the fluorophore fusion orientation alone would determine whether MCP-1 induces dimer association or dissociation. Rather, the dependence of the BRET changes (*i.e.* increase or decrease) on the BRET pair configuration probably reflects structural particularities of the respective pairs studied. Indeed, the specific initial structural state determined by the particular combination of a receptor C terminus fused to either the energy donor or the acceptor could greatly influence how the same conformational switch is sensed by the BRET partners.

Considering the extent of the BRET changes promoted by various ligands for the CXCR4 homodimer, our results seem to contradict the previously reported CXCR4 model proposed by Trent *et al.* (50). In this model, the inverse agonist T140 is predicted to induce only minor rearrangements, whereas more important changes are expected from the binding of the weak agonist AMD3100. It should be pointed out, however, that the model only considered the monomeric form of the receptor; it is perhaps more important that the initial state was assimilated to a fully inactive conformation (based on the available rhodopsin structure (51)). Taking into account the previous report that CXCR4 displays a level of spontaneous activity that can be inhibited by TC14012 but is almost not affected by AMD3100 in cells (42), one could propose that the average basal dimer conformation detected by BRET represents a partially activated conformation that resembles the one stabilized by AMD3100. It follows that AMD3100 would not promote important conformational changes thus only marginally affecting the basal BRET signal, whereas the stabilization of a fully inactive conformation by TC1402 would be translated in considerable BRET changes, which is what we observed in living cells.

In the case of the CXCR4 and CCR2 homodimers, ligand-induced changes in BRET signals nicely parallel the intrinsic efficacy of the ligands; that is, agonists promote signal increases (a full agonist yielding a greater response than a partial agonist) whereas inverse agonists decrease the signal. It would therefore be tempting to speculate that the direction of the BRET changes reflects specific conformational changes that can be directly linked to the signaling efficacy. However, the data obtained with the CXCR4/CCR2 heterodimer questions such a direct relationship. Indeed, the CCR2 agonist MCP-1 either increased or decreased the BRET signal depending on the BRET partner orientation used (see above), demonstrating that the direction of ligand-induced BRET signal inflection may depend on C-terminal structural constraints and thus differ in different systems. It would thus be prudent to conclude that different BRET changes reflect distinct ligand-stabilized receptor conformations but cannot be used to predict intrinsic efficacies. Similar conclusions have already been suggested by other authors (16).

Although no direct relationship between the direction of the BRET changes induced by ligands and their intrinsic efficacies can be strictly established, our data with the CXCR4-derived TM peptides strongly suggest that the conformational changes detected are linked to receptor activity. The original underlying rationale for testing the effect of the inhibitory peptides developed by Tarasova *et al.* (36) was that TM-derived peptides could bind to the protomer interface within dimers, thereby interfering with dimerization and inhibiting receptor activities. Indeed, the activity of a similar peptide has been suggested to result from the disruption of the β2-adrenergic receptor dimers (38), an interpretation that is in line with the proposed roles of TM domains in other GPCR dimer interfaces (52, 53). Hernanz-Falcon *et al.* recently reported that simultaneous mutation of two residues located in the first and fourth TM domains abolished CCR5 dimerization, and that small peptides corresponding to these regions had the same effect (48). On the other hand, it has been proposed that TM-peptides can act by interfering with intramolecular TM packing, thus inducing receptor distortion (54). Our finding that CXCR4 TM-derived peptides did not affect basal BRET levels indicate that they did not function by inhibiting dimerization or by causing major distortion in the initial conformation, because both of these should have caused detectable BRET changes. Our data suggest rather that peptide binding stabilizes the initial conformation hampering the occurrence of any ligand-promoted conformational changes. Given the anti-HIV activity of these peptides (Ref. 36 and data not shown), this interpretation has important implications for the role of CXCR4 in HIV entry, in that it suggests that the peptides could block envelope-induced conformational changes of CXCR4 that are mandatory for viral entry. It remains to be investigated whether the apparently different efficacy of the various peptides to inhibit both function and ligand-promoted conformational changes reflects the respective importance of specific TM domains in the dimerization process.

The observation that CXCR4-derived TM peptides could block the conformational rearrangement of the CXCR4/CCR2 heterodimer promoted by the selective CCR2 agonist MCP-1 provides some clues about the functional organization of chemokine receptor dimers. Indeed, these results demonstrate that the presence of only one selective chemokine is sufficient to change the conformation of the heterodimer. In addition, it is tempting to speculate that conformational changes could be transmitted *in trans* from one protomer to the other. Such interprotomer transmission of conformational changes would suggest that the activity of one receptor could be affected by ligand binding to the other. This type of transactivation has been shown previously for the metabotropic GABAb receptor, where agonist binding to the GABABR1 protomer led to the functional engagement of the heterotrimeric G protein by the GABAbR2 protomer (55, 56). The occurrence of trans-dimer conformational rearrangements could have great impact on the therapeutic use of receptor ligands because they may impinge

not only on the activity of the cognate receptor but also on that of the heterodimer partner. On the other hand, however, our results could also be explained by the capacity of the CXCR4-derived peptides to interfere with CCR2 movements within the heterodimer.

The fact that CXCR4/CCR2 heterodimers are conformationally responsive to selective ligands of either receptor could have potentially important physiological implications. Cell migration frequently involves several chemokines, and the mechanisms leading to the integration of these multiple signals are poorly understood (57–59). Because many chemokine receptors are co-expressed in the same cell types and can be involved together in a single migration process, a role for heterodimers in integrating the multiple signals could be envisioned. For example, CCR2 and CXCR4 have been shown to both contribute to accumulation of activated/memory T-cells in lymph node (60). Whether they play sequential roles or are simultaneously activated, possibly by the intermediate of receptor heterodimers, will require further investigations.

Acknowledgments—We thank Paulo Cordeiro for excellent technical assistance and Marc Parmentier for technical advice.

REFERENCES

1. Terrillon, S., and Bouvier, M. (2004) *EMBO Rep.* **5,** 30–34
2. McVey, M., Ramsay, D., Kellett, E., Rees, S., Wilson, S., Pope, A. J., and Milligan, G. (2001) *J. Biol. Chem.* **276,** 14092–14099
3. Issafras, H., Angers, S., Bulenger, S., Blanpain, C., Parmentier, M., Labbe-Jullie, C., Bouvier, M., and Marullo, S. (2002) *J. Biol. Chem.* **277,** 34666–34673
4. Babcock, G. J., Farzan, M., and Sodroski, J. (2003) *J. Biol. Chem.* **278,** 3378–3385
5. Terrillon, S., Durroux, T., Mouillac, B., Breit, A., Ayoub, M. A., Taulan, M., Jockers, R., Barberis, C., and Bouvier, M. (2003) *Mol. Endocrinol.* **17,** 677–691
6. Canals, M., Marcellino, D., Fanelli, F., Ciruela, F., de Benedetti, P., Goldberg, S. R., Neve, K., Fuxe, K., Agnati, L. F., Woods, A. S., Ferre, S., Lluis, C., Bouvier, M., and Franco, R. (2003) *J. Biol. Chem.* **278,** 46741–46749
7. Gazi, L., Lopez-Gimenez, J. F., Rudiger, M. P., and Strange, P. G. (2003) *Eur. J. Biochem.* **270,** 3928–3938
8. Dinger, M. C., Bader, J. E., Kobor, A. D., Kretzschmar, A. K., and Beck-Sickinger, A. G. (2003) *J. Biol. Chem.* **278,** 10562–10571
9. Kroeger, K. M., Hanyaloglu, A. C., Seeber, R. M., Miles, L. E., and Eidne, K. A. (2001) *J. Biol. Chem.* **276,** 12736–12743
10. Cornea, A., Janovick, J. A., Maya-Nunez, G., and Conn, P. M. (2001) *J. Biol. Chem.* **276,** 2153–2158
11. Wurch, T., Matsumoto, A., and Pauwels, P. J. (2001) *FEBS Lett.* **507,** 109–113
12. Berglund, M. M., Schober, D. A., Esterman, M. A., and Gehlert, D. R. (2003) *J. Pharmacol. Exp. Ther.* **307,** 1120–1126
13. Grant, M., Collier, B., and Kumar, U. (2004) *J. Biol. Chem.* **279,** 36179–36183
14. Cheng, Z. J., and Miller, L. J. (2001) *J. Biol. Chem.* **276,** 48040–48047
15. Latif, R., Graves, P., and Davies, T. F. (2002) *J. Biol. Chem.* **277,** 45059–45067
16. Ayoub, M. A., Couturier, C., Lucas-Meunier, E., Angers, S., Fossier, P., Bouvier, M., and Jockers, R. (2002) *J. Biol. Chem.* **277,** 21522–21528
17. Ayoub, M. A., Levoye, A., Delagrange, P., and Jockers, R. (2004) *Mol. Pharmacol.*
18. Tateyama, M., Abe, H., Nakata, H., Saito, O., and Kubo, Y. (2004) *Nat. Struct. Mol. Biol.* **11,** 637–642
19. Rodriguez-Frade, J. M., Vila-Coro, A. J., de Ana, A. M., Albar, J. P., Martinez, A. C., and Mellado, M. (1999) *Proc. Natl. Acad. Sci. U. S. A.* **96,** 3628–3633
20. Mellado, M., Rodriguez-Frade, J. M., Vila-Coro, A. J., de Ana, A. M., and Martinez, A. C. (1999) *Nature* **400,** 723–724
21. Vila-Coro, A. J., Rodriguez-Frade, J. M., Martin De Ana, A., Moreno-Ortiz, M. C., Martinez, A. C., and Mellado, M. (1999) *FASEB J.* **13,** 1699–1710
22. Mellado, M., Rodriguez-Frade, J. M., Vila-Coro, A. J., Fernandez, S., Martin de Ana, A., Jones, D. R., Toran, J. L., and Martinez, A. C. (2001) *EMBO J.* **20,** 2497–2507
23. Rodriguez-Frade, J. M., Del Real, G., Serrano, A., Hernanz-Falcon, P., Soriano, S. F., Vila-Coro, A. J., De Ana, A. M., Lucas, P., Prieto, I., Martinez, A. C., and Mellado, M. (2004) *EMBO J.* **23,** 66–76
24. Toth, P. T., Ren, D., and Miller, R. J. (2004) *J. Pharmacol. Exp. Ther.* **310,** 8–17
25. Lee, B., Doranz, B. J., Rana, S., Yi, Y., Mellado, M., Frade, J. M., Martinez, A. C., O'Brien, S. J., Dean, M., Collman, R. G., and Doms, R. W. (1998) *J. Virol.* **72,** 7450–7458
26. Smith, M. W., Dean, M., Carrington, M., Winkler, C., Huttley, G. A., Lomb, D. A., Goedert, J. J., O'Brien, T. R., Jacobson, L. P., Kaslow, R., Buchbinder, S., Vittinghoff, E., Vlahov, D., Hoots, K., Hilgartner, M. W., and O'Brien, S. J. (1997) *Science* **277,** 959–965
27. Tang, J., Shelton, B., Makhatadze, N. J., Zhang, Y., Schaen, M., Louie, L. G., Goedert, J. J., Seaberg, E. C., Margolick, J. B., Mellors, J., and Kaslow, R. A. (2002) *J. Virol.* **76,** 662–672
28. Feng, Y., Broder, C. C., Kennedy, P. E., and Berger, E. A. (1996) *Science* **272,** 872–877
29. Murphy, P. M. (2001) *N. Engl. J. Med.* **345,** 833–835
30. Nanki, T., Hayashida, K., El-Gabalawy, H. S., Suson, S., Shi, K., Girschick, H. J., Yavuz, S., and Lipsky, P. E. (2000) *J. Immunol.* **165,** 6590–6598
31. Lukacs, N. W., Berlin, A., Schols, D., Skerlj, R. T., and Bridger, G. J. (2002) *Am. J. Pathol.* **160,** 1353–1360
32. Salcedo, R., and Oppenheim, J. J. (2003) *Microcirculation* **10,** 359–370
33. Lapidot, T. (2001) *Ann. N. Y. Acad. Sci.* **938,** 83–95
34. Charo, I. F., and Peters, W. (2003) *Microcirculation* **10,** 259–264
35. Tamamura, H., Omagari, A., Hiramatsu, K., Gotoh, K., Kanamoto, T., Xu, Y., Kodama, E., Matsuoka, M., Hattori, T., Yamamoto, N., Nakashima, H., Otaka, A., and Fujii, N. (2001) *Bioorg. Med. Chem. Lett.* **11,** 1897–1902
36. Tarasova, N. I., Rice, W. G., and Michejda, C. J. (1999) *J. Biol. Chem.* **274,** 34911–34915
37. Heveker, N., Tissot, M., Thuret, A., Schneider-Mergener, J., Alizon, M., Roch, M., and Marullo, S. (2001) *Mol. Pharmacol.* **59,** 1418–1425
38. Hebert, T. E., Moffett, S., Morello, J. P., Loisel, T. P., Bichet, D. G., Barret, C., and Bouvier, M. (1996) *J. Biol. Chem.* **271,** 16384–16392
39. Mercier, J. F., Salahpour, A., Angers, S., Breit, A., and Bouvier, M. (2002) *J. Biol. Chem.* **277,** 44925–44931
40. Brelot, A., Heveker, N., Montes, M., and Alizon, M. (2000) *J. Biol. Chem.* **275,** 23736–23744
41. Couturier, C., and Jockers, R. (2003) *J. Biol. Chem.* **278,** 26604–26611
42. Zhang, W. B., Navenot, J. M., Haribabu, B., Tamamura, H., Hiramatu, K., Omagari, A., Pei, G., Manfredi, J. P., Fujii, N., Broach, J. R., and Peiper, S. C. (2002) *J. Biol. Chem.* **277,** 24515–24521
43. Gupta, S. K., Pillarisetti, K., Thomas, R. A., and Aiyar, N. (2001) *Immunol. Lett.* **78,** 29–34
44. Hesselgesser, J., Liang, M., Hoxie, J., Greenberg, M., Brass, L. F., Orsini, M. J., Taub, D., and Horuk, R. (1998) *J. Immunol.* **160,** 877–883
45. Haribabu, B., Richardson, R. M., Fisher, I., Sozzani, S., Peiper, S. C., Horuk, R., Ali, H., and Snyderman, R. (1997) *J. Biol. Chem.* **272,** 28726–28731
46. Di Salvo, J., Koch, G. E., Johnson, K. E., Blake, A. D., Daugherty, B. L., DeMartino, J. A., Sirotina-Meisher, A., Liu, Y., Springer, M. S., Cascieri, M. A., and Sullivan, K. A. (2000) *Eur. J. Pharmacol.* **409,** 143–154
47. Doranz, B. J., Orsini, M. J., Turner, J. D., Hoffman, T. L., Berson, J. F., Hoxie, J. A., Peiper, S. C., Brass, L. F., and Doms, R. W. (1999) *J. Virol.* **73,** 2752–2761
48. Hernanz-Falcon, P., Rodriguez-Frade, J. M., Serrano, A., Juan, D., del Sol, A., Soriano, S. F., Roncal, F., Gomez, L., Valencia, A., Martinez, A. C., and Mellado, M. (2004) *Nat. Immunol.* **5,** 216–223
49. Ramsay, D., Kellett, E., McVey, M., Rees, S., and Milligan, G. (2002) *Biochem. J.* **365,** 429–440
50. Trent, J. O., Wang, Z.-x., Murray, J. L., Shao, W., Tamamura, H., Fujii, N., and Peiper, S. C. (2003) *J. Biol. Chem.* **278,** 47136–47144
51. Palczewski, K., Kumasaka, T., Hori, T., Behnke, C. A., Motoshima, H., Fox, B. A., Le Trong, I., Teller, D. C., Okada, T., Stenkamp, R. E., Yamamoto, M., and Miyano, M. (2000) *Science* **289,** 739–745
52. Overton, M. C., and Blumer, K. J. (2002) *J. Biol. Chem.* **277,** 41463–41472
53. Guo, W., Shi, L., and Javitch, J. A. (2003) *J. Biol. Chem.* **278,** 4385–4388
54. George, S. R., Lee, S. P., Varghese, G., Zeman, P. R., Seeman, P., Ng, G. Y. K., and O'Dowd, B. F. (1998) *J. Biol. Chem.* **273,** 30244–30248
55. Galvez, T., Duthey, B., Kniazeff, J., Blahos, J., Rovelli, G., Bettler, B., Prezeau, L., and Pin, J. P. (2001) *EMBO J.* **20,** 2152–2159
56. Kniazeff, J., Galvez, T., Labesse, G., and Pin, J. P. (2002) *J. Neurosci.* **22,** 7352–7361
57. Foxman, E. F., Campbell, J. J., and Butcher, E. C. (1997) *J. Cell Biol.* **139,** 1349–1360
58. Foxman, E. F., Kunkel, E. J., and Butcher, E. C. (1999) *J. Cell Biol.* **147,** 577–588
59. Moser, B., Wolf, M., Walz, A., and Loetscher, P. (2004) *Trends Immunol.* **25,** 75–84
60. Yopp, A. C., Fu, S., Honig, S. M., Randolph, G. J., Ding, Y., Krieger, N. R., and Bromberg, J. S. (2004) *J. Immunol.* **173,** 855–865

Chemokine receptor expression in EBV-associated lymphoproliferation in hu/SCID mice: implications for CXCL12/CXCR4 axis in lymphoma generation

Erich Piovan, Valeria Tosello, Stefano Indraccolo, Anna Cabrelle, Ilenia Baesso, Livio Trentin, Rita Zamarchi, Hirokazu Tamamura, Nobutaka Fujii, Gianpietro Semenzato, Luigi Chieco-Bianchi, and Alberto Amadori

The mechanisms by which intraperitoneal injection of peripheral blood mononuclear cells (PBMCs) from Epstein-Barr virus (EBV)–seropositive donors into severe combined immunodeficient (SCID) mice gives rise to lymphomas (hu/SCID tumors) are far from clear. This study addressed whether chemokine receptors and their ligands could be implicated in this experimental model. CXCR4 was found to be highly expressed in hu/SCID tumors; surface expression of CXCR4 was prevalently limited to a tumor cell subset poorly expressing CD23, whereas the CXCR4 ligand, CXCL12, was predominantly expressed by the tumor subpopulation expressing CD23. In vitro inhibition of this autocrine/paracrine CXCL12/CXCR4 axis significantly inhibited lymphoma proliferation and survival. Furthermore, CXCL12 was expressed in cells recovered from the mouse peritoneal cavity early after PBMC transfer as well as by EBV-transformed B cells but not by resting or activated B lymphocytes; also, lymphoma development was associated with a dramatic increase in the levels of murine CXCL12 present in the peritoneal cavity. Finally, antagonizing the CXCL12/CXCR4 axis in vivo strongly counteracted lymphoma development. These studies demonstrate that CXCL12 expression may be associated with EBV infection and suggest that the CXCR4/CXCL12 axis may participate in the EBV-associated lymphomagenesis process in immunodeficient hosts. (Blood. 2005;105:931-939)

Introduction

Epstein-Barr virus (EBV) is implicated in the pathogenesis of at least 3 malignant disorders of B cells: Burkitt lymphoma, Hodgkin disease, and B-cell lymphoproliferative disease (BLPD) seen in immunosuppressed allograft recipients.[1] The severe combined immunodeficient (SCID) mouse, which lacks functional B and T cells,[2] is a suitable animal model for the study of EBV-associated lymphoproliferation.[3,4] SCID mice injected intraperitoneally with peripheral blood mononuclear cells (PBMCs) from EBV-positive donors develop EBV-positive human B-cell lymphomas (hu/SCID tumors),[4] which display a surface phenotype closely resembling that seen in BLPD with low expression of EBV latent proteins and presenting a mixture of lymphoblastoid and plasmacytoid cells.[5] The events occurring in the peritoneal cavity of PBMC-injected mice are very complex[6] and entail T-cell activation and massive cytokine production, both of which favor the expansion of B lymphocytes, including EBV-positive B-cell precursors. In this regard, we showed that the presence of T lymphocytes within the cellular inoculum is necessary for lymphoma development,[7] and treatment of PBMC-injected mice with cyclosporin A paradoxically counteracts tumor generation.[7,8] Recently, we also demonstrated that no EBV reactivation occurs during the lymphomagenesis process, and tumor masses originate from the expansion of the very few latently infected B lymphocytes present in the inoculum.[9]

Hu/SCID tumors consist of multiple masses at the hepatic hilus, lower splanchnic region, and within the mesenteric tissue,[7] the privileged sites of primary and/or metastatic localization being peritoneum, liver, and lymph nodes. Interestingly, all these organs have been reported to produce high levels of the CXCR4 ligand (CXCL12, previously called stromal cell–derived factor-1 [SDF-1])[10,11]; indeed, no tumor development occurs when PBMCs from EBV-positive donors are injected by other routes,[4] suggesting a critical role of the peritoneal environment for lymphomagenesis. In this regard, it has recently been shown that CXCL12, produced by mesothelial cells lining the peritoneum, is involved in the persistence of peritoneal B lymphocytes in mice[11]; indeed, CXCR4 is expressed on mature B cells.[12]

In view of these observations, we addressed whether chemokine receptors and their ligands could be implicated in EBV-mediated lymphomagenesis in this experimental model. Aims of our study were (1) to define the chemokine receptor expression profile of lymphoblastoid cell lines (LCLs) and hu/SCID tumors; (2) to assess whether chemokines were differentially expressed following cellular transformation by EBV; and (3) to evaluate whether any of the latter could contribute to the outgrowth of EBV-transformed B cells in the immunocompromised host.

From the Department of Oncology and Surgical Sciences, Oncology Section, University of Padua, Italy; Istituto Nazionale per la Ricerca sul Cancro-IST, Genua, Italy; Department of Clinical and Experimental Medicine, Clinical Immunology Branch, University of Padua, Italy; Graduate School of Pharmaceutical Sciences, Kyoto University, Japan; Azienda Ospedaliera Padova, Padua, Italy; and Venetian Institute for Molecular Medicine, Padua, Italy.

Submitted March 2, 2004; accepted September 16, 2004. Prepublished online as *Blood* First Edition Paper, September 28, 2004; DOI 10.1182/blood-2004-03-0799.

Supported in part by grants from Ministero dell'Instruzione, dell' Universitá e della Ricerca (MIUR; FIRB and PRIW and MUIR 60%); Istituto Superiore di Sanità (AIDS Project); Italian Association for Research on Cancer (AIRC) and Italian Foundation for Research on Cancer (FIRC); and Padua University grants. V.T. is a recipient of an AIRC fellowship.

Reprints: Erich Piovan, Department of Oncology and Surgical Sciences, Oncology Section, University of Padua, via Gattamelata 64, Padua, I-35128, Italy; e-mail: erich.piovan@unipd.it.

The publication costs of this article were defrayed in part by page charge payment. Therefore, and solely to indicate this fact, this article is hereby marked "advertisement" in accordance with 18 U.S.C. section 1734.

We report here that lymphoma development in PBMC-injected SCID mice is associated with down-regulated expression by EBV-transformed B cells of the chemokine receptors CCR6, CCR7, and CXCR5, while CXCR3 and CXCR4 are expressed at moderately high levels. We show that most hu/SCID tumors express functional CXCR4 receptors and that CXCL12 affects several biologic responses, including migration, adhesion, proliferation, and invasion. In adjunct, we demonstrate that CXCL12 expression may be related to immortalization of B cells by EBV. We also demonstrate that the hu/SCID tumor subset poorly expressing CD23 expresses functional CXCR4; meanwhile, the tumor subset expressing CD23 is the main producer of CXCL12, suggesting a potential chemotactic loop between these 2 cell populations. Finally, antagonizing the CXCR4/CXCL12 axis through the use of a neutralizing anti-CXCL12 antibody (Ab) or a CXCR4 antagonist was able to counteract lymphoma growth. Because CXCR4 is expressed in the human counterpart of hu/SCID tumors,[13,14] these observations may be relevant to the human setting and open new avenues to therapeutic approaches in B-cell non-Hodgkin lymphomas.

Materials and methods

Isolation of PBMCs and B-cell purification

PBMCs were isolated by Ficoll-Hypaque (Pharmacia Biotech, Uppsala, Sweden) gradient centrifugation as reported elsewhere,[15] washed 4 times with RPMI medium, counted, and used as such for establishment of LCLs and inoculation of SCID mice or separated further. LCLs were generated and maintained as previously reported.[9] Purified B cells were obtained from PBMCs by positive selection using magnetic microbeads (Miltenyi Biotec, Bergisch Gladbach, Germany) according to manufacturer's recommendations.[9] Recovered B cells were of 95% to 98% purity, as determined by flow cytometric analysis. B-cell cultures were set up as previously described.[16]

Generation of human B-cell tumors in SCID mice

SCID mice were purchased from Charles River (Wilmington, MA) and maintained in our animal facilities under pathogen-free conditions. Procedures involving animals and their care conformed with institutional guidelines that comply with national and international laws and policies (European Community EEC Council Directive 86/609, OJ L 358, December 12, 1987). Groups of 7- to 9-week-old SCID mice were injected intraperitoneally with 70×10^6 to 100×10^6 unfractionated PBMCs, observed daily for signs of illness, and killed by cervical dislocation when they became sick. Tumors and other tissues of interest were processed as previously described.[9]

In another set of experiments, hu/SCID tumor cell suspensions were briefly expanded in vitro before being injected intraperitoneally (2×10^6) into SCID mice. Groups of 5 to 8 hu/SCID lymphoma-injected SCID mice were treated with intraperitoneal injections of a polyclonal goat anti-CXCL12 Ab (kindly provided by Prof Robert M. Strieter, UCLA, Los Angeles, CA; 50 μL per mouse per injection); 500 μL of this Ab is sufficient to neutralize 1 μg of either human or murine CXCL12 in leukocyte chemotaxis assays.[17] As controls, we used heat-inactivated goat preimmune serum and phosphate-buffered saline (PBS). The animals were treated every day for 3 weeks starting from the day after tumor injection, and the effects of anti-CXCL12 Ab treatment on lymphoma development were assessed by monitoring survival and histologic examination for evidence of tumor. In other groups of animals (6 to 8 mice) the day before transplantation of lymphoma cells, Alzet pumps (duration 14 days; model 1002, ALZA, Mountain View, CA) containing 50 to 80 mg/mL of the CXCR4-specific antagonist 4F-benzoyl-TN14003[18] or vehicle were implanted subcutaneously. On day 13, the Alzet pumps were replaced with pumps containing the same amounts of peptide or vehicle.

FACS analysis

The following mouse monoclonal antibodies (mAbs) were used: phycoerythrin (PE)–labeled mAb against CCR1 (IgG2a), CCR2 (IgG2a), CCR4 (IgG1), CCR6 (IgG2b), CXCR4 (IgG2b), CXCR5 (IgG2a) (all from R&D Systems, Minneapolis, MN), and CD23 (IgG3; Immunotech, Marseille, France); and fluorescein isothiocyanate (FITC)–labeled mAb to CCR3 (IgG2a), CCR5 (IgG2a), CCR7 (IgG1), CXCR1 (IgG2a), CXCR2 (IgG2a), CXCR3 (IgG1) (all from R&D Systems), and CD23 (IgG1; Becton Dickinson, Mountain View, CA). Irrelevant conjugated mouse Abs of each isotype (Becton Dickinson) were used to establish specificity of staining. The following Abs also were used: rabbit anti-CXCL12 Ab (PeproTech, London, United Kingdom), irrelevant rabbit immunoglobulin G (IgG) (PeproTech), and Alexa 488–labeled goat antirabbit Ab (Molecular Probes, Leiden, The Netherlands). Results were expressed as percent of the cells expressing the relevant marker.

Intracellular expression of CXCL12 in LCLs and hu/SCID tumor cells was detected by flow cytometry as previously described.[19]

Isolation of RNA and RT-PCR

Total RNA was isolated using the RNeasy mini kit (QIAGEN, Hilden, Germany), primed (0.5 to 1 μg) with random hexamers (Promega, Madison, WI), and reverse transcribed. Complementary DNA fragments from the reverse transcriptase (RT) reaction mixture were subjected to polymerase chain reaction (PCR) amplification using AmpliTaq Gold polymerase (Applied Biosystems, Foster City, CA) for 35 to 45 cycles (95°C for 45 seconds, 60°C for 45 seconds, 72°C for 1 minute). The following primers were used: human CXCL12: forward, 5′-ATGAACGCCAAGGTCGTGGTCG-3′, reverse (SDF-1α), 5′-AAGTCCTTTTTGGCTGTTGTGC-3′, or reverse (SDF-1β) 5′-TGACCCTCTCACATCTTGAACC-3′ [20]; human CXCR4: forward, 5′-GGGGATCAGTATATACACTTCAG-3′, reverse, 5′-AGACGCCAACATAGACCAC-3′; mouse CXCL12: forward, 5′-CACCTCGGTGTCCTCTTG-3′, reverse, 5′-GGTCAATGCACACTTGTCTG-3′. For the control of RNA and cDNA preparations, we used RT-PCR for β-actin as previously reported.[21] Amplified products were analyzed on a 1.8% agarose electrophoresis gel and visualized under UV rays after ethidium bromide staining.

In vitro adhesion assays

Adhesion of hu/SCID tumor cells to human umbilical vein endothelial cells (HUVECs) and fibronectin was assayed as previously described,[22,23] with minor modifications. Briefly, hu/SCID tumor cells (1×10^5) were labeled before the assay with the fluorescent dye calcein acetoxymethyl ester (calcein-AM; Molecular Probes) and were subsequently added for 30 to 60 minutes to 96-well culture plates covered by HUVECs, bovine serum albumin (BSA; 40 μg/mL; Sigma, St Louis, MO), or fibronectin (10 μg/mL). After the incubation period, the nonadherent cells were removed by vigorously washing the wells with RPMI 1640 medium (Life Technologies, Grand Island, NY) 3 times. Adherent cells were collected and counted by flow cytometry. A gate was set up using the calcein labeling of the lymphoma cells to exclude HUVECs from the counts. Results were expressed as percentage of adherent cells (ie, number of adherent cells per number of input cells).

For inhibition studies, hu/SCID tumor cells were preincubated with a neutralizing anti-CXCL12 Ab (1:100) or 1 μM TC14012, a CXCR4-specific inhibitor,[24] for 30 minutes at 37°C before being plated in HUVEC- or fibronectin-coated wells.

Chemotaxis and chemoinvasion assay

Migration and invasion were assayed in modified Boyden chambers (Neuro Probe, Gaithersburg, MD) using 13-mm polycarbonate filters of 8-μm pore size as previously described.[25,26] Membranes were uncoated for chemotaxis or coated with 25 μg Matrigel (Becton Dickinson) for invasion assays. The lower compartments were filled with RPMI supplemented with 0.1% BSA with or without CXCL12 (100 to 200 ng/mL). Hu/SCID tumor cells were preincubated for 30 minutes at 37°C in the presence of 1 μM TC14012, anti-CXCL12 Ab, or in control conditions (RPMI–0.1% BSA) and subsequently loaded (3×10^5) onto the upper compartments of the modified

Boyden chambers. After incubation of 2 hours (chemotaxis) or 24 hours (chemoinvasion), the contents of the lower compartments were collected and counted after fixation and staining with crystal violet.

Actin polymerization

To evaluate the effect of CXCL12 on cytoskeleton rearrangement of different tumor subsets, freshly isolated hu/SCID lymphoma cells were labeled with PE-conjugated anti-CD23 mAb at 4°C for 30 minutes. Cells were washed and incubated at 37°C in RPMI medium before assessing cytoskeleton rearrangement. Actin polymerization experiments were performed as previously described.[11]

Proliferation and survival assays

For proliferation and survival studies evaluating the role of endogenous CXCL12, freshly isolated hu/SCID tumor cell suspensions treated with or without anti-CXCL12 Abs (1:20) or TC14012 (50 to 100 μM) were pulsed for 48 hours with 1 μCi [37 Bq] [methyl-^{3}H]thymidine (Amersham, Arlington Heights, IL) or labeled with FITC-conjugated annexin V (PharMingen, BD Biosciences, San Diego, CA) plus propidium iodide (PI; Molecular Probes).[19] Subsequently, thymidine incorporation was evaluated on a scintillation β-plate counter, or the percentage of cells undergoing apoptosis was determined by flow cytometry. Annexin V–positive PI-negative and annexin V–positive PI-positive cells correspond to apoptotic and necrotic cells, respectively.

Confocal microscopy

Confocal microscopic analysis was executed as previously described.[27] Cells were stained with the following primary Abs: mouse anti-CXCR4 mAb (R&D Systems) and rabbit anti–human CXCL12 Ab (PeproTech), while the secondary Abs used were Alexa 594–conjugated anti–mouse Ab (Molecular Probes; red signal) and an Alexa 488–conjugated antirabbit Ab (Molecular Probes; green signal).

Murine CXCL12 ELISA

Peritoneal washings were executed as previously described.[9] For each time point considered, 3 to 5 mice were killed and the liquid obtained from the peritoneal washings of each time point was pooled together. These pools were concentrated 50 times with Centriplus Centrifugal Filter Devices (YM-3; Millipore, Billerica, MA) to obtain a final volume of 300 to 500 μL. The quantity of murine CXCL12 present in the peritoneal washings was then determined using an antibody sandwich enzyme-linked immunosorbent assay (ELISA) (R&D Systems) with a sensibility of more than 44 pg/mL.

Statistical analysis

Results were expressed as mean value ± SD. Statistical analyses of the in vitro data were performed using the nonparametric Mann-Whitney test; in in vivo experiments, Kaplan-Meier survival curves were analyzed with the Mantel-Haenszel test.

Results

EBV transformation of B cells in vitro (LCLs) and in vivo (hu/SCID tumors) is associated with modulation of chemokine receptor expression

The chemokine receptor expression profile of EBV-transformed B cells has not been as yet extensively addressed. Using a panel of mAbs directed against CCR1, CCR2, CCR3, CCR4, CCR5, CCR6, CCR7, CXCR1, CXCR2, CXCR3, CXCR4, and CXCR5, we compared the chemokine receptor expression profile in freshly isolated B lymphocytes, in vitro EBV-immortalized LCL cells, and in vivo–generated hu/SCID tumors. Data are summarized in Figure 1. Circulating B cells expressed CCR6, CCR7, CXCR3, CXCR4, and CXCR5 (Figure 1, circles); very rarely, CCR1, CCR4, CCR5, and CXCR2 were expressed at low levels (data not shown). In contrast, EBV-immortalized LCL cells expressed CCR7, CXCR3, and CXCR4 at a lower level ($P < .05$), with CCR6 and CXCR5 being frequently undetectable (Figure 1, squares); rarely, CCR1, CCR3, and CCR4 were positive at low levels (data not shown). Hu/SCID tumors presented a mixed chemokine receptor expression profile (Figure 1, triangles), with CXCR3 and CXCR4 being substantially expressed, while CCR6, CCR7, and CXCR5 were significantly more weakly expressed compared with freshly isolated B lymphocytes ($P < .05$); rarely, CCR1, CCR2, and CCR4 were positive at low levels (data not shown). In general, a lower percent expression of chemokine receptors was also paralleled by a sizable reduction in mean fluorescence intensity (MFI) of the cells (data not shown). Altogether, these data demonstrate that EBV transformation in vitro is associated with a significant down-regulation of the expression of all chemokine receptors studied (CCR6, CCR7, CXCR3, CXCR4, and CXCR5); on the contrary, EBV-positive hu/SCID tumors generated after PBMC transfer into SCID mice continue to express substantial levels of CXCR3 and CXCR4, comparable to those present in freshly isolated B cells, though down-modulating CCR6, CCR7, and CXCR5.

CXCR4 is functional and is predominantly expressed by a CD23^{low} hu/SCID tumor cell population

The functionality of the chemokine receptors expressed on hu/SCID tumor cells was evaluated by a chemotaxis assay. In most cases CXCL12 gave the greatest chemotactic response (data not shown), and because tumors in our experimental model consist of multiple peritoneal masses with frequent involvement of liver, spleen, and abdominal lymph nodes, sites known to produce high levels of CXCL12,[10] subsequent experiments focused on the CXCL12/CXCR4 axis. As shown in Figure 2A, chemotaxis to

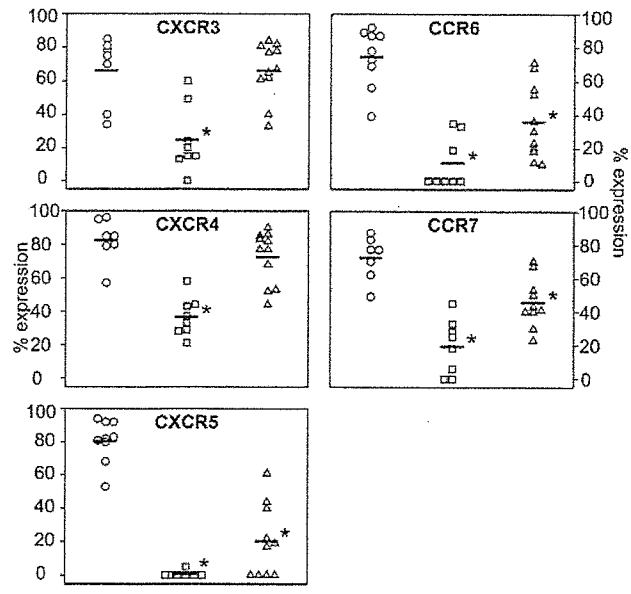

Figure 1. Modulation of chemokine receptor expression in EBV-transformed B cells in vitro (LCLs) and in vivo (hu/SCID tumors). Flow cytometric analysis for CCR6, CCR7, CXCR3, CXCR4, and CXCR5 expression on B lymphocytes (○), LCL cells (□), and freshly isolated hu/SCID tumor cells (△). Each point shows the percentage of cells expressing the indicated chemokine receptor. Horizontal bars represent the mean value of each group; the asterisks denote a significant difference compared with B cells ($P < .05$).

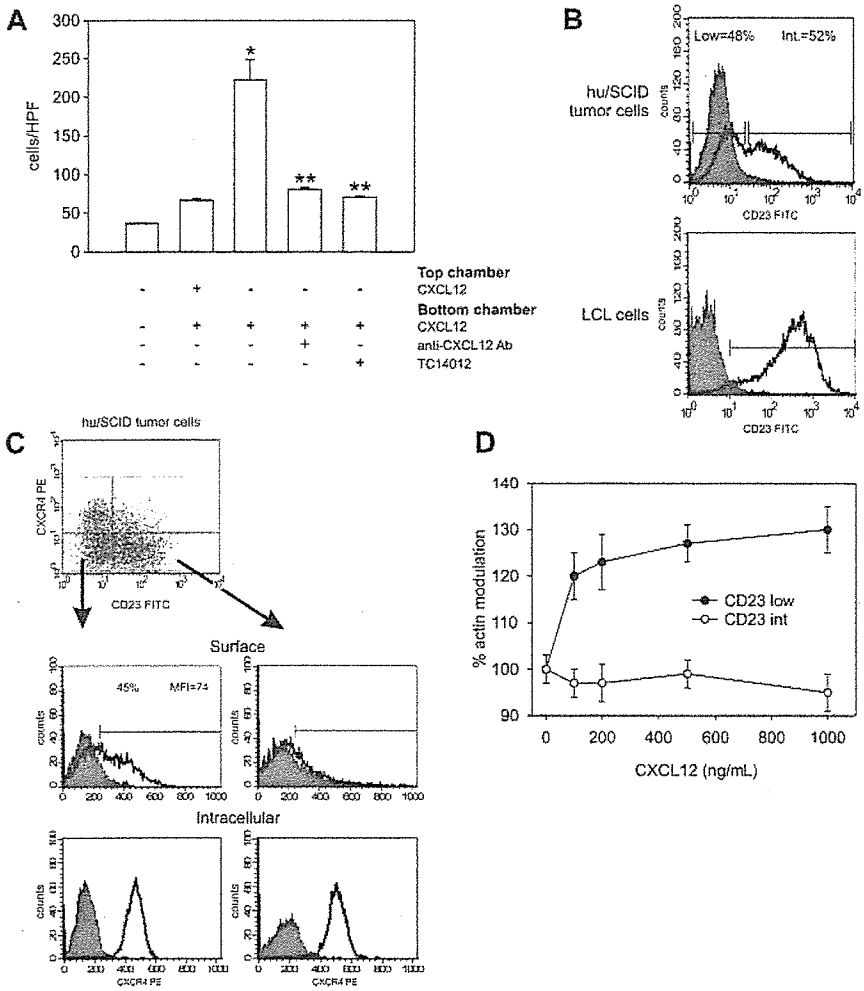

Figure 2. CXCR4 is functional, and its surface expression segregates with B-cell phenotype in hu/SCID tumor cells. (A) Effect of CXCL12 on migration of hu/SCID lymphoma cells. Lymphoma cells were added to the chemotaxis chamber in the presence (+) or absence (−) of the following reagents: 100 ng/mL CXCL12 (SDF-1α), neutralizing anti-CXCL12 Abs (1:100), and TC14012 (1 and 5 μM). Migrated cells were recovered from the lower chamber after 2 hours at 37°C and counted. Results are the mean of 2 separate experiments executed in triplicate (± SD). The single asterisk denotes a significant difference compared with untreated cells ($P < .05$); 2 asterisks denote a significant inhibition by TC14012 or anti-CXCL12 Abs of the chemotactic properties of CXCL12-stimulated cells ($P < .05$). (B) Tumor cells were stained with the FITC-conjugated anti-CD23 mAb and the PE-conjugated anti-CXCR4 mAb before being analyzed by cytofluorimetry. The fluorograms represent the expression pattern of CD23 in a representative hu/SCID tumor sample (top) and LCL cells (bottom). (C) The expression of surface and intracellular CXCR4 (upper and lower panels, respectively) in the $CD23^{low}$ (left diagrams) and $CD23^{int}$ (right diagrams) tumor cell subsets is shown. A representative experiment of 3 consecutive experiments is shown. (D) Effect of CXCL12 on actin polymerization in the 2 hu/SCID lymphoma cell subsets. Lymphoma cells were labeled with PE-conjugated anti-CD23 Ab and tested by flow cytometry for CXCL12-induced cytoskeleton rearrangement. Results (mean ± SD from 2 experiments) show the kinetics of actin polymerization following addition of different concentrations of CXCL12; 100% corresponds to the baseline level.

CXCL12 could be significantly blocked by pretreatment of cells with neutralizing Abs to CXCL12 and the CXCR4 antagonist TC14012. Further, no significant increase of migration was observed with a uniform distribution of CXCL12, indicating that this is a gradient-dependent chemotactic response. It has been reported that hu/SCID tumors are composed of 2 phenotypically distinct B-cell subsets: $CD23^{low}$ (and $CD38^{high}$ [$CD38^{hi}$]) and $CD23^{intermediate}$ ([$CD23^{int}$] and $CD38^{int}$), demonstrated to harbor a different EBV gene expression profile[5]; on the other hand, LCL cells have been reported to be homogenously $CD23^{hi}CD38^{int/low}$ and only show a reduced CD23 expression when transferred into SCID mice.[5,28] We thus investigated whether CXCR4 expression on hu/SCID tumor cells was segregated with the B-cell phenotype. To analyze the coexpression of membrane CXCR4 and CD23 on hu/SCID tumors, the tumor cells were examined cytometrically after staining with FITC anti-CD23 and PE anti-CXCR4 mAbs. As shown in Figure 2B (upper panel), in agreement with previously published data,[5] within hu/SCID tumor cells 2 cell subpopulations were discernable on the basis of CD23 expression, one $CD23^{low}$ and one $CD23^{int}$; this was not the case for LCLs, where virtually all cells showed high CD23 expression (Figure 2B, lower panel). Further, a clear segregation in CXCR4 expression was observed in the 2 hu/SCID tumor cell subpopulations (Figure 2C), with CXCR4 surface expression being predominantly confined to the $CD23^{low}$ subset (Figure 2C, top left panel). On the other hand, both tumor cell subsets expressed consistent levels of internal CXCR4 (Figure 2C). To determine the functional relevance of the generation of the 2 cell subsets, we investigated F-actin modulation following incubation with increasing concentrations of CXCL12. As shown in Figure 2D, a significant increase in F-actin polymerization could be observed only in the $CD23^{low}$ tumor subset, suggesting that this subset is the main responder to CXCL12.

The CXCR4 ligand, CXCL12, is expressed by LCLs and a CD23-expressing hu/SCID tumor cell population but not resting or activated B cells

EBV-transformed B lymphocytes have a propensity to produce autocrine factors for their own growth and survival.[29,30] We evaluated by both RT-PCR and fluorescence-activated cell sorter (FACS) analysis whether LCLs and hu/SCID tumors expressed the CXCR4 ligand, CXCL12, thus possibly activating an autocrine loop; indeed, this has not been investigated so far. As shown in Figure 3A, all LCLs (lanes 1 to 5) and hu/SCID tumor cells (lanes 6 to 10) tested expressed mRNA for SDF-1α/CXCL12 and most also expressed SDF-1β/CXCL12 (data not shown), with the α isoform being the predominant transcript in most cases. To investigate whether the expression of CXCL12 by LCLs and hu/SCID tumor cells was simply associated to the activation state of these cells or more strictly linked to EBV transformation, B cells were purified and stimulated in vitro with anti-CD40 mAb and interleukin-4 (IL-4) for 3 to 5 days. RT-PCR analysis of these samples disclosed that no specific transcripts for SDF-1α/CXCL12 or SDF-1β/CXCL12 could be evidenced in both freshly isolated (Figure 3A,

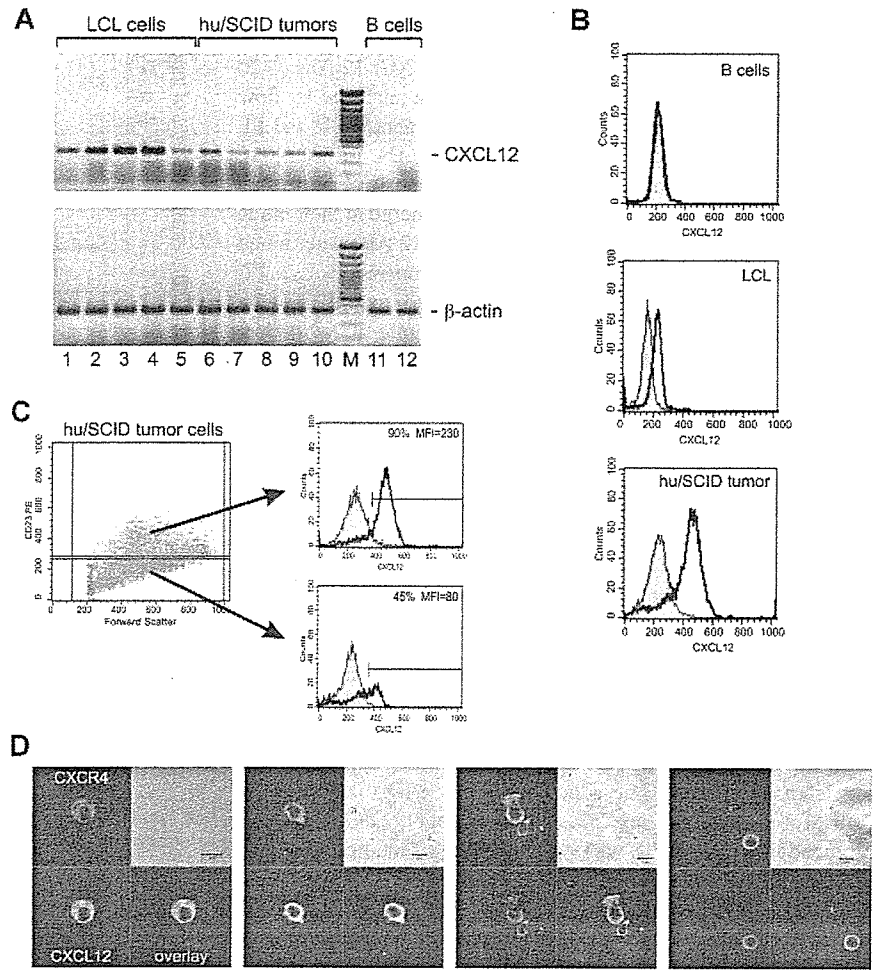

Figure 3. CXCL12 expression in EBV-transformed B cells and its segregation with B-cell phenotype. (A) The expression of CXCL12 and β-actin in LCL cells and hu/SCID tumor cells was evaluated by RT-PCR. Representative results from 5 LCLs and 5 hu/SCID tumors are shown. Lane M corresponds to 50-bp molecular weight marker. Lanes 12 and 13 correspond to a representative case of purified resting B cells and to the same B cells after 48 hours of in vitro stimulation with anti-CD40/IL-4, respectively. (B-C) The intracellular expression of CXCL12 in LCL cells and hu/SCID tumor cells was evaluated by cytofluorimetric analysis. (B) The fluorograms (from top to bottom) show normal B cells not expressing CXCL12, LCL cells, and hu/SCID tumor cells. (C) The expression of CXCL12 in the $CD23^{low}$ (lower right) and $CD23^{int}$ (upper right) tumor cell subsets is shown. A representative experiment of 3 consecutive experiments is shown. (D) Confocal microscopic analysis evaluating the coexpression of surface CXCR4 and intracellular CXCL12 in hu/SCID tumors. Cells were fixed, stained with anti-CXCR4 Ab, and subsequently permeabilized before incubation with anti-CXCL12 Ab. The signal for CXCR4 is shown in red, while the CXCL12 signal is in green. Areas of colocalization are shown in yellow.

lane 11 of each panel) and in vitro–activated B cells (Figure 3A, lane 12 of each panel), thus showing that CXCL12 expression was in some way associated with EBV immortalization. The expression of CXCL12 in EBV-transformed B cells was also confirmed at the protein level by cytofluorimetric analysis of both LCLs and hu/SCID tumors (Figure 3B); interestingly, CXCL12 was shown to be preferentially produced by the CD23-expressing (LCL-like) subset of hu/SCID tumors (Figure 3C). To better document the segregation of CXCR4 and CXCL12 expression in hu/SCID tumors, we executed confocal microscopy analysis at the single cell level after staining the cells for surface CXCR4 and intracellular CXCL12. As shown in Figure 3D, on the whole, cells expressing high levels of surface CXCR4 (red signal) expressed much more weakly CXCL12 (green signal) compared with the cell population expressing CXCR4 weakly or not at all.

In vitro CXCL12 neutralization inhibits hu/SCID lymphoma cell proliferation and survival

We showed thus far that hu/SCID tumors express CXCL12 and that they can efficiently respond to exogenous CXCL12. We thus set out to investigate the possible functional role of endogenous CXCL12 on hu/SCID cell biology. We first investigated whether CXCL12 neutralization by the use of anti-CXCL12 neutralizing Abs or the use of a recently described specific blocking agent for CXCR4,[24] such as TC14012, affected lymphoma growth in vitro. Indeed, as shown in Figure 4A, treatment of ex vivo–obtained lymphoma cells for 2 days with neutralizing anti-CXCL12 Abs (1:20 dilution) or TC14012 (50 to 100 μM) significantly reduced lymphoma cell proliferation ($P < .05$). On the other hand, the goat preimmune serum used as control at the same dilution did not significantly alter lymphoma proliferation (Figure 4A). We next tested the effect of

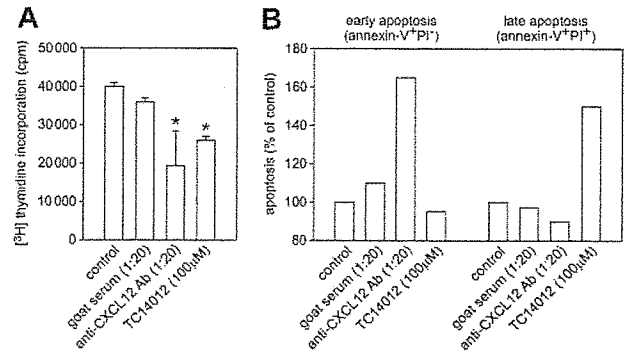

Figure 4. Effect of in vitro neutralization of CXCL12 and CXCR4 on hu/SCID lymphoma cell proliferation and survival. (A) Ex vivo–obtained hu/SCID lymphoma cells were cultured for 48 hours with or without TC14012 (50 to 100 μM), neutralizing anti-CXCL12 Abs (1:20), or appropriate controls. Each result is representative of the mean counts per minute (cpm) ± SD of triplicate wells after a 48-hour pulse with [methyl-^{3}H]thymidine. This analysis is representative of 3 separate experiments with different tumors with similar results; the single asterisk denotes a significant difference compared with untreated cells ($P < .05$). (B) Ex vivo–obtained hu/SCID lymphoma cells were cultured for 48 hours with or without TC14012 (50 to 100 μM), neutralizing anti-CXCL12 Abs (1:20), or appropriate controls. Cells were then harvested and labeled with PI and FITC-conjugated annexin V before being analyzed by flow cytometry. Data are shown as the mean percent change relative to control. One representative experiment of 3 performed is shown.

blocking the endogenous CXCL12 on apoptosis of hu/SCID lymphoma cells. To this end, ex vivo–obtained lymphoma cells were treated for 2 days with neutralizing anti-CXCL12 Abs (1:20 dilution) or TC14012 (50 to 100 μM) and then analyzed by flow cytometry after staining with FITC-conjugated annexin V and PI. Treatment of cells with either anti-CXCL12 Abs or TC14012 determined a significant increase in annexin V–positive cells (data not shown). However, a difference seemed to emerge in their mode of action, because the neutralizing anti-CXCL12 Abs determined mainly an increase in early apoptosis (annexin V–positive PI-negative), while the CXCR4 antagonist acted mainly on late apoptosis (annexin V–positive PI-positive) (Figure 4C). Notably, the concentrations of the neutralizing anti-CXCL12 Abs (1:100 dilution) or TC14012 (1 to 5 μM) used in functional assays such as chemotaxis, adhesion, or chemoinvasion did not affect either the proliferation or survival of lymphoma cells (data not shown). On the whole, these data suggest that survival and proliferation of hu/SCID tumors are in part mediated by CXCL12/CXCR4 interactions and autocrine secretion of CXCL12.

CXCL12 stimulates the adhesive and invasive properties of hu/SCID tumor cells

CXCL12 has been reported to regulate the function of several integrins on normal human hematopoietic cells[31]; we thus investigated whether CXCL12 also regulated integrin activity in hu/SCID tumor cells. As shown in Figure 5A, CXCL12 consistently increased the adhesion of hu/SCID tumor cells to both fibronectin (Figure 5A, middle panel) and HUVECs (Figure 5A, right panel), whereas it did not affect their adhesion to BSA (Figure 5A, left panel).

Because tumor cell invasion is one of the major characteristics of malignant cells, we evaluated this feature using a chemoinvasion Matrigel assay. As shown in Figure 5B, the invasive capability of hu/SCID tumors was increased in the presence of a CXCL12 gradient (Figure 5B, open columns). In addition, TC14012 significantly inhibited both the adhesive and invasive properties of these cells (Figure 5, gray columns), thus indicating that the invasion-promoting effect of CXCL12 was a specific phenomenon; similar results were obtained when neutralizing anti-CXCL12 Abs were used (data not shown).

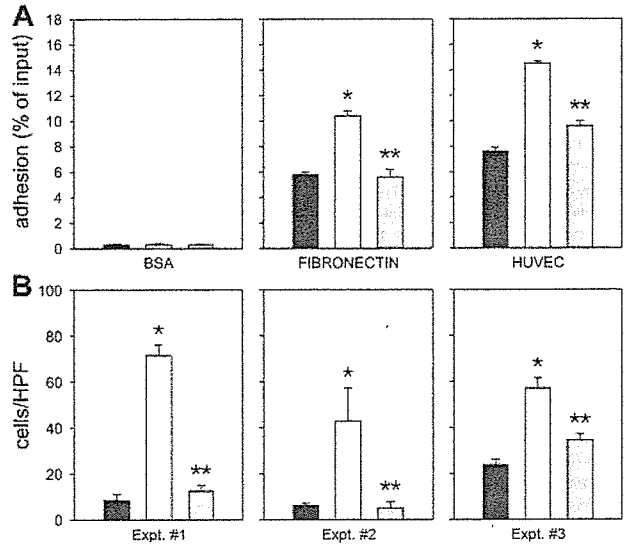

Figure 5. Effect of CXCL12 on the adhesive and invasive properties of hu/SCID tumor cells. (A) Effect of CXCL12 on adhesion of hu/SCID tumor cells to fibronectin and endothelial cells. The panels from left to right represent adhesion of hu/SCID tumor cells to bovine serum albumin (BSA), fibronectin, and HUVECs. Unstimulated cells are shown as black bars; open and gray bars represent hu/SCID tumor cells stimulated with CXCL12/SDF-1α (200 ng/mL) in the absence and in the presence, respectively, of the CXCR4 antagonist TC14012. Data are shown as mean ± SEM of 2 consecutive experiments; the single asterisk denotes a significant difference compared with untreated cells ($P < .05$); 2 asterisks denote a significant inhibition by TC14012 of the adhesive properties of CXCL12-stimulated cells ($P < .05$). (B) Cells invading the Matrigel were collected from the lower compartments and counted as detailed in "Materials and methods"; results are expressed as number of cells per high power field (HPF) and represent mean values ± SEM of 3 replicate determinations for each tumor. Hu/SCID lymphoma cells showed significant invasion through Matrigel toward a CXCL12 gradient (open columns); this phenomenon was inhibited by treating the cells with TC14012 (gray columns). The single asterisk denotes a significant difference ($P < .05$) compared with unstimulated cells; 2 asterisks denote a significant inhibition by TC14012 of the invasive properties of CXCL12-stimulated cells ($P < .05$). Results obtained in 3 different hu/SCID tumor masses representative of 4 consecutive experiments are shown.

CXCL12 is expressed in vivo during the early phases of EBV-mediated lymphomagenesis, and its neutralization inhibits tumor growth in vivo

We finally directly addressed the possible relevance of the CXCL12/CXCR4 axis in the lymphomagenesis process of this experimental model. To this end, we first wondered whether CXCL12 and CXCR4 were indeed expressed in the mouse peritoneal microenvironment. Thus, cells were recovered from the peritoneal cavity of SCID mice at 4, 8, and 16 days following intraperitoneal transfer of PBMCs from EBV-positive donors, and the expression of human and murine CXCL12 and human CXCR4 was determined by RT-PCR. In addition, the peritoneal washings were evaluated for the presence of murine CXCL12 by ELISA. We used primers specific for murine and human CXCL12 (Figure 6A), because under our experimental conditions a band corresponding to human CXCL12 could only be evidenced on human cells but not on murine tissues (Figure 6A). At the same time, primers specific for murine CXCL12 gave a band only when mouse tissues were used (Figure 6A). As shown in Figure 6B, both human and mouse CXCL12 transcripts were undetectable in PBMCs immediately prior to injection; meanwhile, they were both readily evidenced in the cell populations recovered at all the time points considered. On the other hand, the CXCR4 transcript was always consistently detected in all cell populations studied (Figure 6B).

RT-PCR results seemed to indicate that murine CXCL12 is the main isoform present in the early stages of lymphomagenesis. We thus determined whether murine CXCL12 protein was effectively present in the peritoneal cavity and how it varied during the lymphomagenesis process. As shown in Figure 6C, low levels of murine CXCL12 were present in the peritoneal washings prior to PBMC injection; however, during the course of the lymphomagenesis process there was a considerable increase in the protein levels of CXCL12, reaching a peak at the moment of killing.

In view of these data, which suggested the possibility that a CXCL12/CXCR4 autocrine/paracrine loop could be at work in lymphoma development and progression, we wondered whether interfering with the CXCL12/CXCR4 axis could affect lymphoma development in SCID mice. To this end, we chose to use freshly obtained hu/SCID tumor cell suspensions to generate tumors in naive SCID mice. Hu/SCID lymphoma cells were used instead of PBMCs from EBV-positive donors because of the well-known problem of the very high heterogeneity in the generation of lymphomas in SCID mice among different donors,[32,33] which would have complicated the interpretation of the effects of

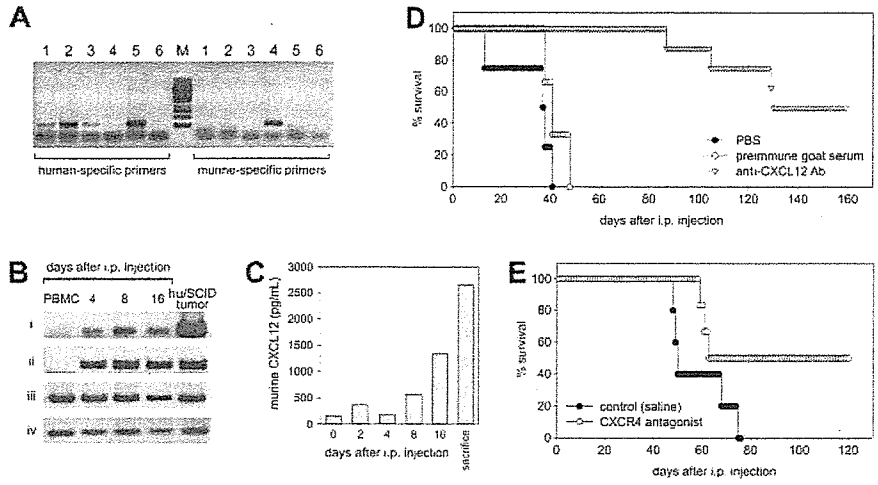

Figure 6. Expression of the CXCL12/CXCR4 axis in vivo following PBMC transfer to SCID mice and effects of CXCL12 and CXCR4 neutralization in vivo. (A) The specificity of our primer pairs for human and murine CXCL12 was evaluated on human and murine samples. A band corresponding to human CXCL12 was detected only on human samples: HUVECs (lane 1), MRC-5 (lane 2), human microvascular endothelial cells (lane 3), and LCLs (lane 5) but not on murine tissues such as the peritoneal membrane (lane 4). Conversely, primers specific for murine CXCL12 gave a band only on murine tissues (lane 4). Lane 6 corresponds to the water control. (B) The expression of CXCL12 and CXCR4 in cells recovered from the peritoneal cavity of SCID mice injected with PBMCs from EBV-positive donors was evaluated by RT-PCR. The cells were analyzed before and after various time intervals following intraperitoneal injection for the expression of human CXCL12 (i), murine CXCL12 (ii), human CXCR4 (iii), and β-actin (iv). The first left lane corresponds to the profile obtained with freshly isolated PBMCs; the last lane corresponds to a hu/SCID tumor sample. (C) Expression of murine CXCL12 as evaluated by ELISA in the peritoneal washings obtained at various time intervals following PBMC transfer in SCID mice. (D-E) Effect of CXCL12 and CXCR4 neutralization on tumor growth. Freshly isolated hu/SCID tumor cell suspensions were injected intraperitoneally into naive SCID mice. (D) Mice were treated with intraperitoneal injections of goat anti-CXCL12 Ab, PBS, or heat-inactivated goat preimmune serum every day for 3 weeks starting from the day after cell transfer. The effect of anti-CXCL12 Ab and treatment on lymphoma development was assessed by effects on survival. Five to 8 mice were included in each experimental group, and the experiment was repeated twice. (E) In another group of animals following PBMC transfer, Alzet pumps releasing the CXCR4 antagonist 4F-benzoyl-TN14003 were implanted subcutaneously and changed every 2 weeks for a total of 2 implants. The effect of treatment with 4F-benzoyl-TN14003 on lymphoma development was assessed by effects on survival and tumor dissemination. Six to 8 mice were included in each experimental group.

neutralization of the CXCR4/CXCL12 axis on lymphoma development. Hu/SCID tumor-injected mice were then treated with intraperitoneal injections of a neutralizing anti-CXCL12 Ab or adequate controls. For CXCR4 neutralization, 4F-benzoyl-TN14003, a recently reported T140 derivative shown to have an increased biostability with respect to TC14012,[18] was administered by subcutaneous injection using Alzet pumps beginning from the day preceding transplantation of hu/SCID lymphoma cells for 4 consecutive weeks. As shown in Figure 6D, in experiments evaluating the effect of CXCL12 neutralization, all control animals succumbed within 50 days after tumor cell transfer; meanwhile, mouse treatment with the neutralizing anti-CXCL12 Ab significantly delayed lymphoma development (Figure 6D; $P < .0002$), with 50% of anti-CXCL12–treated animals being tumor free after 180 days. A similar effect on animal survival was observed when 4F-benzoyl-TN14003 was used (Figure 6E; $P < .05$).

Discussion

In this article we addressed the contribution of the chemokine system to the outgrowth of EBV-positive B-cell lymphomas in SCID mice injected intraperitoneally with PBMCs from EBV-positive donors. We showed that most in vitro–transformed LCLs strongly down-regulated the expression of most chemokine receptors, compared with normal B lymphocytes; meanwhile, most hu/SCID tumors analyzed expressed CXCR3 and CXCR4 at moderately high levels and CCR6, CCR7, and CXCR5 at intermediate/low levels. That in vivo and in vitro immortalization of circulating B cells by EBV is associated with down-regulation of CCR6, CCR7, and CXCR5 expression may be partially linked to the activation state of these cells.[34] Our data concerning LCLs partially confirm those recently reported by other workers,[35] in that we also found a down-regulation of CXCR4 and CXCR5; however, we were not able to document any significant up-regulation of CCR6 surface expression in LCL cells. Notably, only a few LCL samples were considered by these authors[35]; in addition, the modulation of chemokine receptor expression (in comparison with a single peripheral blood B-cell sample examined) was solely based on a semiquantitative RT-PCR analysis,[35] while our conclusions are based on protein expression by cytofluorimetry on a much larger number of samples. On the other hand, this apparent discrepancy might depend on the very high heterogeneity between LCLs, as also encountered in the present study (Figure 1), and the modulation of some chemokine receptors associated with in vitro culture (data not shown). The differential profile of chemokine receptor expression between LCLs and hu/SCID tumor cells, with these latter expressing moderately high CXCR3 and CXCR4 levels, may also partially reflect a different stage of maturation of these 2 cell populations.[28] It is well known that plasma cells express CXCR4 while down-modulating CCR7 and CXCR5,[36] whereas activated B cells down-modulate CCR6 (Brandes et al[34] and data not shown). Thus, the down-regulation of CCR6, CCR7, and CXCR5 seen in hu/SCID tumors may partially reflect their stage of differentiation and their activation state.

Recently, it has been described that EBV latent genes can also modify chemokine receptor expression.[35] Hu/SCID tumors in general exibit low levels of latent EBV transcripts such as Epstein-Barr nuclear antigen-1 (EBNA-1), EBNA-2, and latent membrane protein-1 (LMP-1) with respect to LCLs.[5] Thus, differential expression of EBV latent genes between LCLs and hu/SCID tumors may also help explain the differences in the chemokine receptor profile between LCLs and hu/SCID tumors. In this regard, as outlined previously and reported by others,[5,28] hu/SCID tumors are composed of 2 phenotypically distinct B-cell subsets: $CD23^{low}CD38^{hi}$ and $CD23^{int}CD38^{int}$; meanwhile, LCLs have been